ASTROBIOLOGY
Volume 14, Number 2, 2014

DOI: 10.1089/ast.2013.0990

Using Dimers to Measure Biosignatures and Atmospheric Pressure for Terrestrial Exoplanets

Amit Misra,[1,2,3] Victoria Meadows,[1,2,3] Mark Claire,[4,2,5] and Dave Crisp[6,2]

Abstract

We present a new method to probe atmospheric pressure on Earth-like planets using (O_2-O_2) dimers in the near-infrared. We also show that dimer features could be the most readily detectable biosignatures for Earth-like atmospheres and may even be detectable in transit transmission with the James Webb Space Telescope (JWST). The absorption by dimers changes more rapidly with pressure and density than that of monomers and can therefore provide additional information about atmospheric pressures. By comparing the absorption strengths of rotational and vibrational features to the absorption strengths of dimer features, we show that in some cases it may be possible to estimate the pressure at the reflecting surface of a planet. This method is demonstrated by using the O_2 A band and the 1.06 μm dimer feature, either in transmission or reflected spectra. It works best for planets around M dwarfs with atmospheric pressures between 0.1 and 10 bar and for O_2 volume mixing ratios above 50% of Earth's present-day level. Furthermore, unlike observations of Rayleigh scattering, this method can be used at wavelengths longer than 0.6 μm and is therefore potentially applicable, although challenging, to near-term planet characterization missions such as JWST. We also performed detectability studies for JWST transit transmission spectroscopy and found that the 1.06 and 1.27 μm dimer features could be detectable (SNR > 3) for an Earth analogue orbiting an M5V star at a distance of 5 pc. The detection of these features could provide a constraint on the atmospheric pressure of an exoplanet and serve as biosignatures for oxygenic photosynthesis. We calculated the required signal-to-noise ratios to detect and characterize O_2 monomer and dimer features in direct imaging–reflected spectra and found that signal-to-noise ratios greater than 10 at a spectral resolving power of $R = 100$ would be required. Key Words: Remote sensing—Extrasolar terrestrial planets—Habitability—Radiative transfer—Biosignatures. Astrobiology 14, 67–86.

1. Introduction

Atmospheric pressure is a fundamental parameter for characterizing the environment and habitability of an extrasolar planet. Water's stability on a planetary surface as a liquid depends on both the surface temperature and pressure. While the freezing point of water is not strongly dependent on pressure, pressure does affect water's boiling point and sublimation. Thus, a reliable estimate of the surface pressure is an important part of the measurement suite required to determine the habitability of an exoplanet.

Despite the importance of atmospheric pressure, current proposed methods for measuring pressure by using remote-sensing techniques that could be applicable to exoplanetary atmospheres are challenging. The existing techniques include the use of Rayleigh scattering (Kasting and Traub, 2010) or the widths of individual absorption lines (Kaplan *et al.,* 1964; Gray, 1966) or absorption bands (Chamberlain *et al.,* 2006; Spiga *et al.,* 2007; Ignatiev *et al.,* 2009; Chamberlain *et al.,* 2013). The presence and location of a blue Rayleigh scattering tail in a spectrum can provide information about the existence and pressure of an atmosphere. However, strong blue absorbers in the atmosphere (*e.g.,* O_3, SO_2, NO_2, and many others) or surface features can mask this tail (Crow *et al.,* 2011). Furthermore, the Rayleigh scattering tail is most prominent shortward of 0.6 μm, below the short wavelength cutoff of the James Webb Space Telescope (JWST) (Gardner *et al.,* 2006).

[1]University of Washington Astronomy Department, Seattle, Washington, USA.
[2]NAI Virtual Planetary Laboratory, Seattle, Washington, USA.
[3]University of Washington Astrobiology Program, Seattle, Washington, USA.
[4]Department of Earth and Environmental Sciences, University of St Andrews, Fife, Scotland.
[5]Blue Marble Space Institute of Science, Seattle, Washington, USA.
[6]Jet Propulsion Laboratory, California Institute of Technology, Pasadena, California, USA.

Lastly, planets around M dwarfs are likely to be the first to be characterized (Deming *et al.,* 2009), and M dwarfs have relatively less visible-flux to Rayleigh scatter than solar-type stars. The Rayleigh tail would be more difficult to detect and characterize for planets orbiting stars of this stellar class.

It is also possible to use the widths of absorption features to estimate pressure. Pressure increases the widths of vibration rotation lines of gases. This method has been successful for Earth when using high-resolution spectra of the O_2 A band (Barton and Scott, 1986; Mitchell and O'Brien, 1987; Crisp *et al.,* 2012), for Mars with CO_2 features near 2 μm (Gray, 1966; Chamberlain *et al.,* 2006; Forget *et al.,* 2007; Spiga *et al.,* 2007), and for the cloud tops of Venus with the 1.6 μm CO_2 band (Ignatiev *et al.,* 2009). This method provides unambiguous results when the spectral resolution is sufficiently high to resolve the profiles of individual spectral lines. It can also be used at lower spectral resolution but requires prior knowledge of the mixing ratio of the absorbing gas.

Here, we explore the feasibility of a new method to directly measure the pressure of an Earth-like atmosphere that combines the absorption features of dimers with those of monomer vibration-rotation bands to yield estimates of the atmospheric pressures even when the mixing ratio of the monomer is uncertain. Previous pressure estimates for which dimer absorption was used have been made for the cloud tops of Earth, but these techniques have required prior knowledge of the gas mixing ratio profile (Acarreta *et al.,* 2004). Dimers are bound or quasi-bound states between two molecules driven together by molecular interactions. For example, the O_2-O_2 or O_4 dimer consists of two O_2 molecules temporarily bound to each other by Van der Waals forces. This dimer has its own rotational and vibrational modes and produces spectral features distinct from its constituent O_2 monomers. Additionally, absorption from dimer molecules is more sensitive to pressure than that of monomers. The optical depth (how much absorption occurs) for dimers and monomers can be expressed by the following equations:

$$d\tau_{\text{monomer}} = \sigma \rho dl = \sigma P/T dl \quad (1)$$

$$d\tau_{\text{dimer}} = k\rho^2 dl = kP^2/T^2 dl \quad (2)$$

where $d\tau_{\text{monomer}}$ and $d\tau_{\text{dimer}}$ are the monomer and dimer differential optical depths, σ is the monomer cross section, ρ is the number density of the gas, k is the dimer cross section, P is the pressure, T is the temperature, and dl is the path length. While the monomer (*e.g.,* O_2) optical depth is directly proportional to pressure, the optical depth of the dimer (*e.g.,* O_2-O_2) is dependent on the square of the density (and hence square of the pressure). This difference in pressure dependence allows us to estimate atmospheric pressure by comparing the dimer and monomer absorption features

For an oxygen-rich, Earth-like atmosphere, the best combination of bands to use for pressure determination at near-infrared wavelengths (>0.6 μm) would be the (O_2) A band at 0.76 μm and the 1.06 μm O_4 dimer band. The 0.76 μm O_2 A band is the strongest O_2 feature in the visible–near-infrared spectral region and is found in a relatively clean region of the spectrum between two water vapor bands. We have chosen the dimer feature at 1.06 μm as the likely best option, due to its combination of band strength and its location in a relatively uncluttered region of the planetary spectrum. Other O_4 features overlap with water features (dimer feature between 5.5 and 7 μm) or O_2 vibration-rotation bands (0.63, 0.76, and 1.27 μm dimer features) or are weaker than the 1.06 μm dimer feature (0.477 and 0.57 μm dimer features). Nevertheless, some other features, in particular the strong 1.27 μm feature, could be used if the 1.06 μm dimer feature is not detectable.

In the proposed technique, the O_2 0.76 μm (monomer) band is used to provide an estimate of the atmospheric concentration of O_2 and combined with the O_4 1.06 μm (dimer) band to constrain the atmospheric pressure. This method can be used with either transmission spectroscopy or directly detected reflection or emission spectra, and serves as a complement to pressure determination techniques such as Rayleigh scattering, which only work in the visible. Although the proof of concept is shown here with oxygen, this technique is not limited to the oxygen dimer in an Earth-like atmosphere in the visible to near-infrared. The same technique is applicable to pairs of monomer and dimer absorption features across a wider range of planetary atmospheric composition and spectral wavelength range.

2. Methods

In the present study, we generated transit transmission and direct imaging reflected spectra for cloud- and aerosol-free Earth-like exoplanets. The models we used to do this are described below.

2.1. Transmission spectroscopy model

2.1.1. Model overview. When an extrasolar planet transits or occults its host star, the planetary atmosphere is backlit, and some of the star's light traverses the planet's atmosphere on limb trajectories. This transmitted light can be used to characterize the planet's atmosphere (Seager and Sasselov, 2000; Brown, 2001; Hubbard *et al.,* 2001). This has been done for a number of Jupiter- and Neptune-sized planets (*e.g.,* Charbonneau *et al.,* 2002; Vidal-Madjar *et al.,* 2003; Pont *et al.,* 2008) and the super-Earth/mini-Neptune GJ 1214 b (*e.g.,* Bean *et al.,* 2010).

The transmission spectroscopy model used here is based on Spectral Mapping Atmospheric Radiative Transfer (SMART) (Meadows and Crisp, 1996; Crisp, 1997), which is a spectrum-resolving (line-by-line), multi-stream, multiple-scattering radiative transfer model. We modified SMART to generate transit transmission spectra by combining the monochromatic absorption and scattering opacities for each atmospheric layer calculated by SMART with the limb path lengths inherent in a transit transmission event. The transmission model included gas absorption, Rayleigh scattering, interaction-induced absorption, extinction from clouds and aerosols, refraction, and limb darkening. Because multiple scattering was not included in the transit transmission component of the model, we considered only cloud- and aerosol-free atmospheres for this work.

2.1.2. Refraction. An important characteristic of the transit transmission spectroscopy model is the inclusion of

refraction. As described by García Muñoz *et al.* (2012), refraction sets a fundamental limit on the range of pressures that can be probed during a transit, independent of absorption and scattering. Light refracts as it passes through an atmosphere, with a larger refraction angle as higher pressures and densities are probed. For every planet-star system, there will be a maximum tangent pressure in the planet's atmosphere that can be probed, because at greater pressures the light will be refracted by too large of an angle to be able to reach a distant observer during the transit.

For each tangent height in each atmosphere, we calculated the total angle of refraction for a beam of light emitted from the host star, using a modified version of the method described by Auer and Standish (2000). Their method was developed for calculating refraction for astronomical observations on Earth given a tangent altitude, apparent zenith angle, and an atmospheric density profile. We calculated the angle of refraction over a range of zenith angles to determine whether a path exists to connect the host star to a distant observer via the planetary atmosphere. Transit transmission spectroscopy cannot probe the tangent altitudes at which no such path exists.

The radius of the star, planet-star distance, and composition of the planet's atmosphere determine the maximum tangent pressure. The radius of the star and planet-star distance control the apparent angular size of the star from the planet's perspective. The larger the angular size, the greater the range of pressures that can be probed. For an Earth analogue orbiting a Sun-like star, the angular size of the star is $\sim 0.5°$, while for an Earth analogue orbiting an M5 dwarf and receiving the same total flux, the angular size of the star is $\sim 2°$. Therefore, transit transmission spectroscopy can probe higher pressures, that is, see deeper into the atmosphere, for the planet orbiting an M dwarf. Figure 1 shows this effect by comparing all possible paths at one tangent height for a planet around an M dwarf and a planet around a Sun-like star, with each planet receiving the same total flux.

The composition of the atmosphere determines the refractivity (index of refraction -1) of the atmosphere. Atmospheres with greater refractivities will have lower maximum tangent pressures. The refractivity at standard temperature and pressure can vary from ~ 1.5 times the refractivity of air for CO_2 to slightly less than half the refractivity of air for H_2, when considering only the common bulk atmospheric gases in the solar system. Therefore, in general it will be possible to probe higher pressures for an H_2 atmosphere than a CO_2 or air atmosphere.

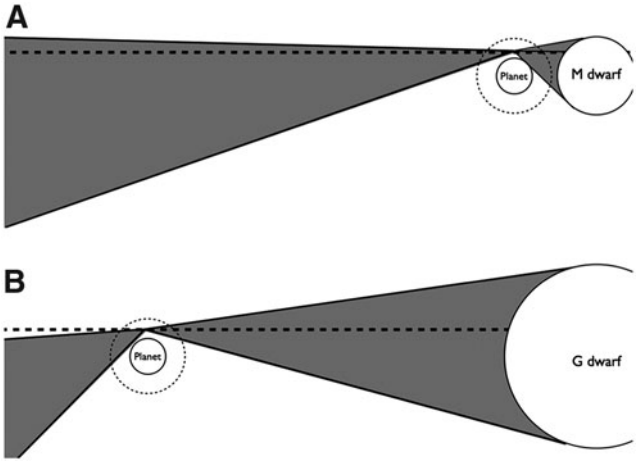

FIG. 1. Comparison of the effect of refraction on (**A**) an exoplanet around an M dwarf and (**B**) a planet around a Sun-like star with both planets receiving the same total flux. The dashed circles are the planetary atmospheres. The solid lines represent different refracted paths through the atmosphere, and the dashed lines are the hypothetical paths to a distant observer observing the planet in transit transmission. Only paths that lie exactly on that dashed line will be observed. For the M dwarf case, there will be a path connecting the star to the observer through the atmosphere at this particular tangent height. However, there is no path in the Sun-like star case. This means that a transit transmission spectrum of the planet around the M dwarf can theoretically probe higher pressures of the atmosphere than in the Sun-like star case.

2.2. Direct imaging (reflected) spectroscopy model

The reflected spectra were generated with the standard version of SMART, which can include multiple scattering from clouds and aerosols. However, to maintain consistency with the transmission spectrum model, clouds were not included in this study. The reflected spectra were generated assuming a surface with a constant albedo of 0.16, which is the average albedo of the cloud-free Earth (Pierrehumbert, 2010). We also assumed the surface is a Lambertian scatterer. Other surface types could have introduced an error into any quantitative estimates in this paper, unless explicitly included in a retrieval attempt. Figure 2 shows the wavelength dependence of a variety of surface types from the Advanced Spaceborne Thermal Emission and Reflection Radiometer (ASTER) spectral library (Baldridge *et al.,* 2009) and the United States Geological Survey (USGS) digital spectral library (Clark *et al.,* 2007). Surface albedos are nearly constant in the bands considered here, though, for example, snow fluctuates by $\sim 20\%$ within the 1.06 μm dimer band. We modeled a test case with SMART with the snow surface to determine the error different surfaces can introduce. We found a difference of 15% between the seawater and snow cases when measuring the equivalent width (defined in Section 2.4) of the 1.06 μm dimer band. This difference was significantly less than the difference in measured equivalent widths for the cases considered in this paper. Therefore, we considered any discrepancies due to variations in surface albedo to be minimal for the present work.

2.3. Model inputs

2.3.1. Model atmospheres. The cloud-free model atmospheres were generated by a one-dimensional (altitude) photochemical code with an extensive history in early Earth (Zerkle *et al.,* 2012), modern Earth (Catling *et al.,* 2010), and exoplanet (Domagal-Goldman *et al.,* 2011) research. The planetary radius and surface gravity used were the radius of Earth (6371 km) and surface gravity of Earth ($9.87\ m/s^2$). The vertical grid consists of 200 plane-parallel layers that are each 0.5 km thick in altitude, in which radiative transfer, atmospheric transport, and photochemical production and loss are solved simultaneously, subject to upper (stellar flux, atmospheric escape) and lower

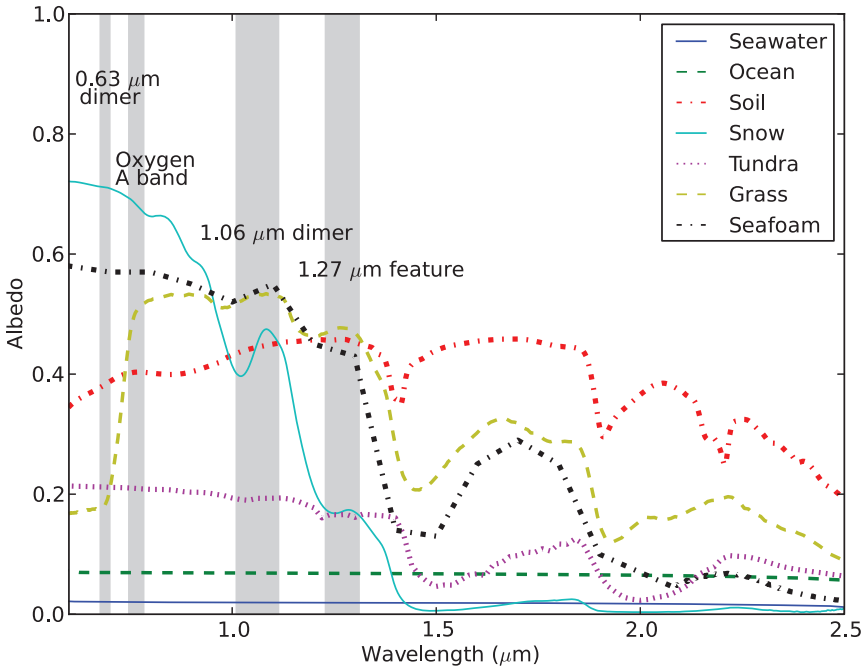

FIG. 2. Wavelength-dependent albedos for a variety of surfaces. The shaded regions correspond to O_2 monomer and dimer bands. For any absorption band, as long as the albedo does not vary widely within the band's wavelength range, it should be possible to measure an accurate equivalent width for each feature. The maximum variation within a band is no more than ~20%. Therefore, we do not consider surface albedo variations important for this work. (Color graphics available online at www.liebertonline.com/ast)

(volcanoes and biology) boundary conditions. The model calculates the mixing ratios of each species in each layer by solving the coupled mass-continuity/flux equations with the reverse Euler method (appropriate for stiff systems) and a variable time-stepping algorithm. Dimer concentrations were computed by using estimations from quantum mechanical calculations. First, we fit the temperature dependence of the equilibrium constant for O_2 dimer formation using the following equations:

$$Kp = (p(O_2)_2/(pO_2)^2/\text{atm}^{-1} \quad (3)$$

$$Kp(T) = 2428 * T^{(-3.518)} \quad (4)$$

where $p(O_2)_2$ and pO_2 are the dimer and monomer partial pressures and T is the temperature (Uhlik *et al.,* 1993). The dimer mixing ratio was then computed as

$$p(O_2)_2 = Kp(T) * (pO_2)^2 * P \quad (5)$$

where P is the pressure in atmospheres. The choice of quantum parameters in our fit of Eq. 4 ensures that our calculation is a lower limit to the dimer concentrations, an assumption which matches modern atmospheric data well (Slanina *et al.,* 1994).

The model atmospheres used in this study started with boundary conditions that reproduce Earth's modern atmospheric chemistry. We then replaced the solar spectrum with the M dwarf spectrum described in 2.3.3 and decreased the surface albedo to 0.16 to account for cloud-free conditions. This ''modified Earth around an M dwarf'' model was then perturbed to examine changes to both total pressure and oxygen concentrations. Total atmospheric pressures of 0.1, 0.5, 1.0, 3.0, 5.0, and 10.0 bar were examined. At each of these total pressures, lower boundary conditions on O_2 mixing ratios were set at 0.1, 0.5, 1.0, and 2.0 times Earth's present level. This corresponds to oxygen mixing ratios from 2% to 42%, which is roughly the range of oxygen concentrations experienced throughout the past 2.5 billion years of Earth's history (Kump, 2008). Boundary conditions for all other species were held fixed at modern values. Figure 3 shows the pressure-temperature profile and volume mixing ratio profiles for the 1.0 times the present atmospheric level (PAL) O_2 cases for spectrally active gases in the wavelength region examined here. Stable steady-state solutions were analyzed in all but the three cases with the highest O_2 surface partial pressures. For those three cases, we extrapolated from our converged results at lower O_2 mixing ratios by increasing O_2 concentrations, scaling the dimer concentrations with the square of the O_2 mixing ratio, and keeping all other gas mixing ratios constant.

For all tests presented here, we assumed Earth-like temperature and water vapor profiles, precluding the need for costly climate simulations. More specifically, we took the modern Earth temperature profile as a function of altitude and computed the corresponding pressure levels assuming hydrostatic equilibrium. This simplification provides a useful baseline but limits the range of validity of these results somewhat because the gas absorption cross sections and number densities depend on these atmospheric properties. The impact of this assumption is assessed in Section 3.4. For pressure/temperature regions corresponding to Earth's mesosphere, we adopted a temperature of 180 K, which likely overestimates the temperature in these regions. Dimer absorption preferentially occurs in higher-pressure regions and so is insensitive to assumed conditions in the tenuous upper atmosphere. Our model grid was capped at 100 km altitude, ensuring optically thin conditions for nearly all species, and made allowances for CO_2 and N_2 photolysis above the upper boundary. We used the modern measured eddy-diffusion profile to simulate convective motion for all atmospheres regardless of pressure. While this simplification would affect the prediction of trace gas concentrations, all species

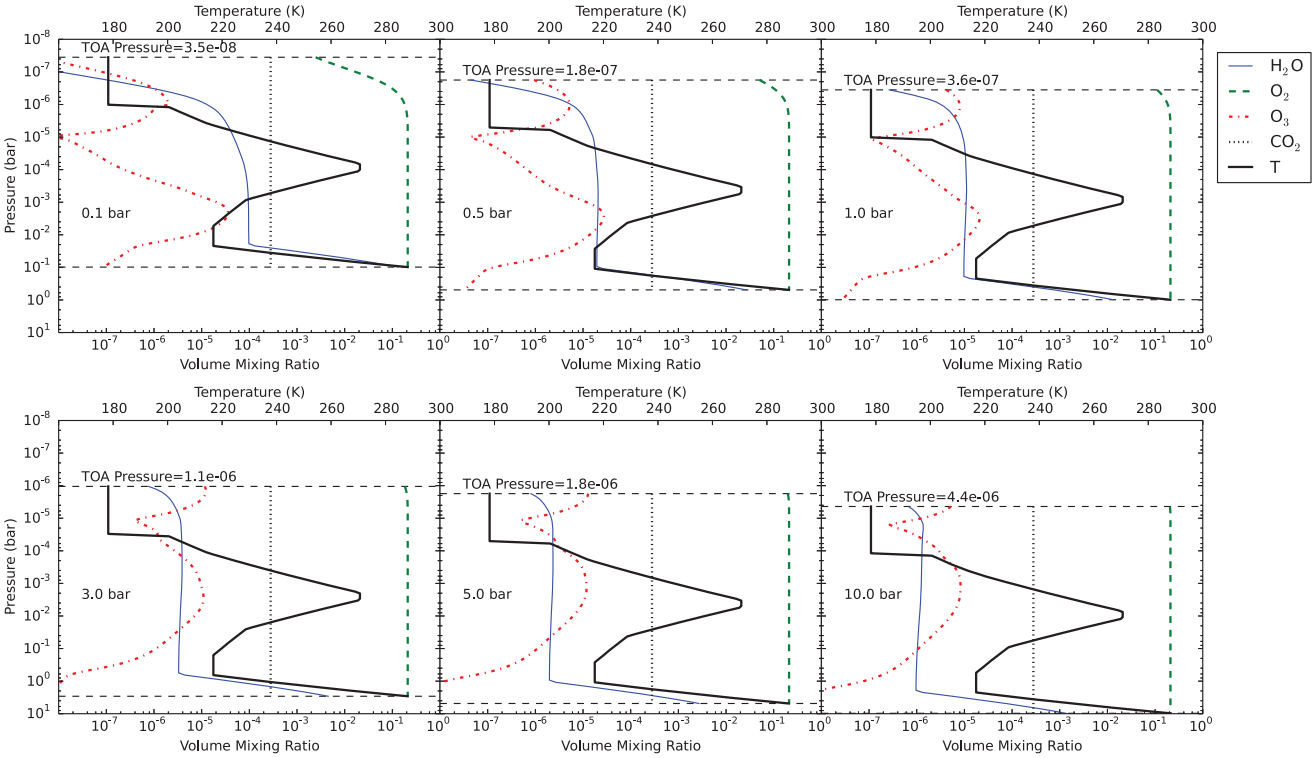

FIG. 3. Pressure-temperature profiles and volume mixing ratio profiles for all pressures at $1.0\times$PAL O_2. The black dashed lines represent the surface pressures and top-of-atmosphere (TOA) pressures. We use the modern Earth temperature-altitude profile in all cases and calculate the pressures assuming hydrostatic equilibrium. The remainder of the atmosphere is N_2 for all cases. (Color graphics available online at www.liebertonline.com/ast)

analyzed here are either well-mixed (CO_2, O_2, N_2) or short-lived (dimers) so are not sensitive to changes in turbulent mixing.

2.3.2. Absorption line lists and cross sections. We used the HITRAN 2008 database line lists (Rothman *et al.,* 2009) to generate opacities in SMART. The dimer absorption cross sections for O_2 were taken from Greenblatt *et al.* (1990) and Maté *et al.* (1999).

2.3.3. Stellar properties. In the present study, we assumed that the planet orbits an M5V star, or an M dwarf with stellar radius of 0.20 R_{sol} and a luminosity of 0.0022 L_{sol} (Kaltenegger and Traub, 2009). The planet was placed at a distance of 0.047 AU so that the total integrated incoming stellar flux was equal to the total flux Earth receives from the Sun today. An M5 dwarf was chosen for these tests because there is a high probability that the terrestrial planets that will be the most easily characterized in the near future will be orbiting this class of star (Deming *et al.,* 2009). Additionally, transit transmission spectroscopy can probe pressures up to the $\sim$1 bar level in an atmosphere for an Earth analogue around an M dwarf, while for the Earth around the Sun, it can only probe pressures as great as $\sim$0.2 bar. At these pressures and lower, the 1.06 μm dimer feature is very weak, even at 200% PAL O_2. Thus, using Earth-like atmospheres around an M dwarf instead of around the Sun provides a better demonstration of the pressure dependence of dimer features.

To simulate the spectrum of the star, we used a Phoenix NextGen synthetic spectrum (Hauschildt *et al.,* 1999) for all wavelengths greater than $\sim$300 nm. For the shorter wavelengths, we used the UV spectrum of AD Leo (Segura *et al.,* 2005). The Phoenix spectrum was normalized so that the total integrated flux was equal to 1373 W/m^2, which is the integrated flux Earth receives from the Sun. The AD Leo spectrum from Segura *et al.* (2005) was left unchanged, as it was already normalized to equal the amount of flux a planet near the inner edge of the habitable zone would receive.

2.3.4. Spectral resolution. We used a spectral resolving power of 100 to provide relevance to JWST, which will provide new opportunities for characterizing the atmospheres of transiting exoplanets (Lafreniere *et al.,* 2013). Once JWST is launched, the Near-Infrared Spectrograph (NIRSpec) will provide spectra with a spectral resolving power ($R = \frac{\lambda}{\Delta\lambda}$) of $\sim$100 between 0.6 and 5.0 μm in single prism mode (Köhler *et al.,* 2005). We examine the effect of varying the spectral resolution in Sections 3.6 and 4.3.

2.4. Absorption strength measurements

To make a quantitative estimate of absorption strengths, we measured equivalent widths for the reflected spectra and measured part-per-million differences in flux for the transmission spectra. Equivalent widths were calculated with the following equation:

$$W = \int (1 - F_\lambda / F_0) d\lambda \qquad (6)$$

where W is the equivalent width, F_λ is the flux at each wavelength λ, and F_0 is the continuum flux at each wavelength. To obtain the equivalent widths, we first measured the area of the spectral band below the continuum. For each absorption band, we define the continuum by hand. For the O_2 A band, the continuum was assumed to be linear with wavelength; and for the 1.06 μm feature, the continuum was assumed to be constant with wavelength because in several of the cases the continuum at the longer wavelengths was difficult to define due to H_2O absorption. The equivalent width is the width, in units of wavelength, of a rectangle measured from the continuum to the level of zero flux with the same total area as the spectral band. We could not use this type of measurement for the transmission spectra because of the difficulty in defining the zero flux level. Therefore, we quantified the absorption strengths for the transmission spectra by measuring the change in flux from the continuum to the point of greatest absorption within a band.

2.5. Detectability calculations

We performed detectability studies (Deming *et al.,* 2009; Kaltenegger and Traub, 2009; Belu *et al.,* 2011; Rauer *et al.,* 2011) for the model spectra, assuming the exoplanet-star system is at a distance of 5 pc. We calculated the expected signal-to-noise ratio (SNR_{star}) using the JWST Exposure Time Calculator (ETC)[1]. The JWST ETC includes background noise from sky, dark, thermal, and zodiacal sources along with read-out noise and photon noise. The estimates provided are expected to be within 20% of the mission requirements. We note that for all the cases considered, the noise is dominated by photon noise. We do not include noise from detector intrapixel variations (Deming *et al.,* 2009), but in principle calibration time could be devoted to mapping the pixels, as has been done with Spitzer Space Telescope Infrared Array Camera (Carey *et al.,* 2012). We also note that noise levels within $\sim$20% of the photon noise limit have been obtained for transit transmission spectra with the Hubble Space Telescope in spatial scan mode, wherein the target star is trailed during each exposure by telescope motion perpendicular to the direction of dispersion (Deming *et al.,* 2013; Wakeford *et al.,* 2013). Spatial scan mode is being considered for JWST; so assuming photon-limited noise in our calculations, while optimistic, provides a reasonable estimate of the detectability of absorption features (Drake Deming, private communication, October 13, 2013).

We assumed that every possible transit is observed in JWST's 5-year mission lifetime, ignoring decreases in integration time due to non-zero impact parameters (where the planet does not traverse the center of the stellar disk and therefore has a lower transit duration) and limits on visibility based on the ecliptic latitude of the exoplanet (see Belu *et al.,* 2011). For the Earth-Sun analogue, this corresponds to a total integration time of $\sim 2.3 * 10^5$ s, and for the Earth-M5V analogue, an integration time of $\sim 10^6$ s. We normalize the solar spectrum (using the Phoenix G2V model available on the site) to a Johnson V magnitude of 3.32 and the M5V spectrum to $2.1 * 10^{-13}$ erg cm^{-2} s^{-1} Å^{-1} at 1 μm.

At each wavelength within an absorption band, we measured the signal as the magnitude of the difference from the continuum flux. The noise is expressed in parts per million (ppm, $10^6/SNR_{star}$) at each wavelength. The final SNR of the transit transmission spectrum is the square root of the sum of the squares of the SNR at each wavelength in the absorption band divided by $\sqrt{2}$, which is included because the transit transmission spectrum must be calibrated against the out-of-transit spectrum of the star.

We also performed detectability studies for the direct imaging reflected spectra that could be relevant to proposed direct imaging planet detection and characterization missions. For these calculations, we did not use an instrument simulator because the exact specifications for these missions are not currently defined. For each absorption band, we calculated two SNRs, one for detecting the spectral feature (SNR_D) and one for measuring the flux at the center of the band to a precision of 3σ (SNR_P). We calculated two SNRs because obtaining information about pressure from a spectral feature requires more than detection; it also requires a quantitative estimate of the strength of that spectral feature. To calculate SNR_D, we divided the reflected flux by the stellar flux, defined a continuum, and calculated the signal as the difference between the continuum and the normalized reflected flux. We assumed the noise is constant over the entire absorption band and then calculated the noise level required to detect the spectral feature with a SNR_{band} of 3 in the absorption band. The final SNR_D is the mean of the continuum reflected flux level divided by the calculated noise. To calculate SNR_P, we selected the wavelength within the band with the lowest radiance. We set the value of a second noise level as the lowest radiance divided by 3. SNR_P is the continuum flux level divided by the noise required to obtain a SNR of 3 at the lowest radiance in the absorption band.

3. Results

3.1. Transit transmission spectra

We generated transit transmission spectra and direct imaging spectra for atmospheres with O_2 concentrations of 10%, 50%, 100%, and 200% PAL and pressures of 0.1, 0.5, 1, 3, 5, and 10 bar. Figure 4 shows the resulting transit transmission spectra for 100% PAL O_2. Transmission spectra of atmospheres with pressures $\geq$1 bar are nearly identical for a given O_2 concentration because refraction limits depth of penetration to $<$1 bar. The dimer feature is weak for the 0.1 and 0.5 bar cases.

Figures 5, 6, and 7 show the resulting transit transmission spectra for O_2 concentrations of 10%, 50%, and 200% PAL. The 1.06 μm dimer feature is very weak at all pressures for O_2 concentrations at 10% PAL and weak for 50% PAL O_2, while it is very strong for pressures above 0.1 bar at 200% PAL O_2.

3.2. Reflected spectra

Figure 8 shows the reflected spectra for modern O_2 mixing ratios in atmospheres with a range of total pressure from 0.1 to 10 bar. The 0.5 and 5.0 bar cases are omitted

[1]http://jwstetc.stsci.edu.

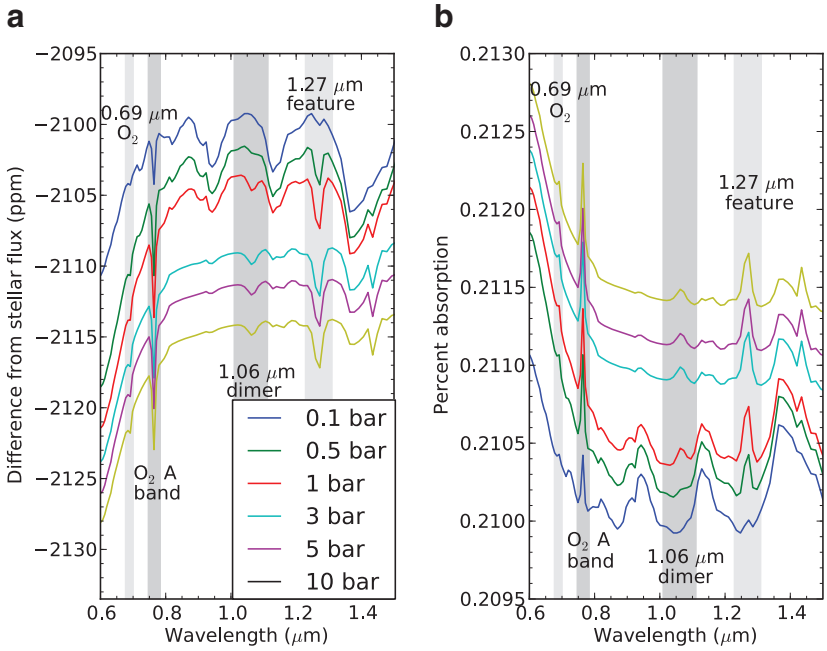

FIG. 4. Transmission spectra of an Earth-like atmosphere with different total atmospheric pressures. (**a**) Difference in flux from the stellar flux. (**b**) Percent of stellar flux absorbed by the atmosphere. The 1.06 μm dimer feature is strong only in the spectra corresponding to atmospheric pressures greater than $\sim$0.5 bar. The spectra for atmospheres with pressure $\geq$1 bar are nearly identical except for an offset because there is a fundamental limit on which heights in an atmosphere can be probed by transmission spectroscopy. For an Earth-like atmosphere around the M5V used here, only the top 0.9 bar can be probed for all atmospheres at all wavelengths. This pressure corresponds to an altitude of $\sim$1 km above the surface for a 1 bar atmosphere and 19 km above the surface for a 10 bar atmosphere. The offset is due to the flux blocked by layers in the atmosphere with pressure greater than 0.9 bar.

from the plots to increase clarity but are still included in the equivalent width and SNR calculations. The 1.06 μm dimer feature is extremely weak for the present-day atmosphere, but in contrast to its behavior in the transmission spectra, it is a very prominent feature for the 3, 5, and 10 bar atmospheres.

Figures 9, 10, and 11 show the reflected spectra at pressures between 0.1 and 10 bar for 10%, 50%, and 200% PAL O_2, respectively. In the 10% PAL case, the O_2 dimer feature at 1.06 μm is very weak because the total amount of O_2 is very low, even for a 10 bar atmosphere. The 1.06 μm dimer feature is stronger in the 3, 5, and 10 bar cases for atmospheres with 50% PAL O_2. Finally for the 200% O_2 atmospheres, the 1.06 μm dimer feature is one of the strongest spectral features, even in the 1 bar atmosphere.

3.3. Quantitative absorption measurements

Figure 12 shows the flux change for the transmission spectra and equivalent widths for reflected spectra at different pressures and O_2 concentrations for the O_2 A band and the 1.06 μm dimer feature. For a given O_2 concentration, the transit transmission flux differences for the O_2 A band are roughly constant for pressures $\geq$1 bar due to refraction. The 1.06 μm dimer feature flux differences increase slightly with pressure but are also constant for pressures $\geq$1 bar for a given O_2 concentration. The dimer

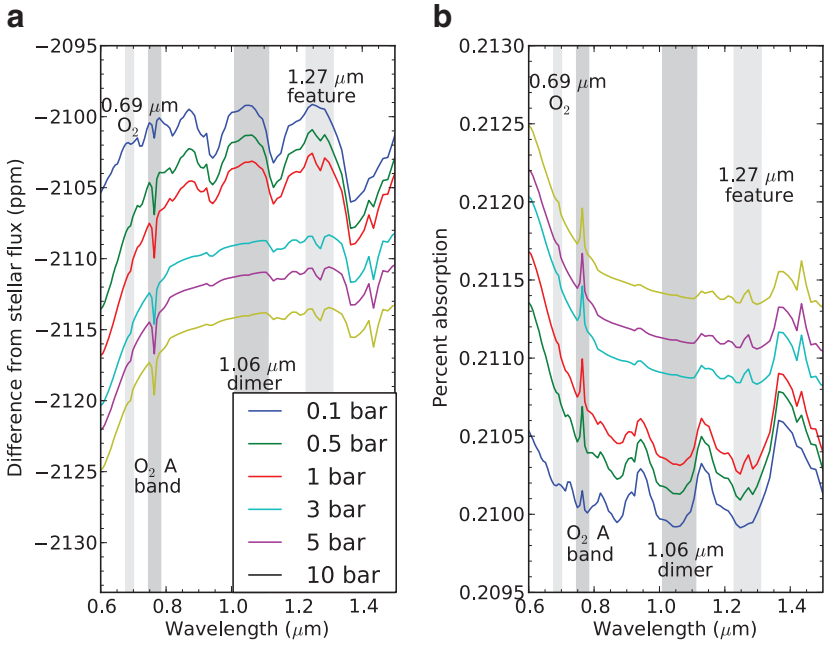

FIG. 5. Same as Fig. 4 but for 10% of the present-day level of O_2. The dimer features do not appear at all because the O_2 concentration is too low.

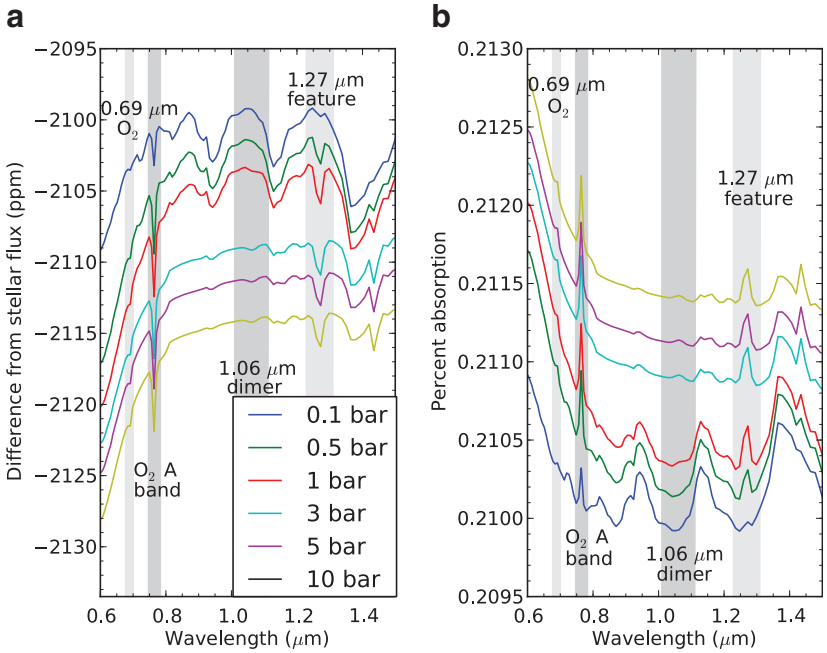

FIG. 6. Same as Fig. 4 but for 50% of the present-day level of O_2. The 1.06 μm dimer feature is very weak and is still weak for the highest surface-pressure atmospheres. (Color graphics available online at www.liebertonline.com/ast)

feature does not appear in transmission for cases with 10% PAL O_2.

For the direct imaging (reflected) spectra, both the O_2 A band and 1.06 μm dimer feature equivalent widths increase with pressure and increased O_2 concentrations. However, the dimer feature equivalent widths are much more sensitive to pressure. At higher pressures, the dimer feature is strong except for cases with 10% PAL O_2, in which the 1.06 μm dimer feature is too weak to quantify.

Figures 13–15 show the relationships between the quantitative absorption measurements described above and atmospheric quantities including the O_2 mixing ratio and the O_2 partial pressure at the surface. The part-per-million flux difference measured in transit transmission for the O_2 A band could be used to constrain the O_2 mixing ratio, as shown in Fig. 13b. The O_2 partial pressure at the surface can be estimated by using the ratio between the 1.06 μm dimer and O_2 A band absorption measurements. These ratios are shown in Fig. 13a with part-per-million flux differences and in Fig. 14 with equivalent widths. The O_2 mixing ratio and O_2 partial pressure at the surface can be combined to provide a unique estimate of the surface pressure of the planet. A more detailed description of the pressure measurement technique is given in Section 4.1.

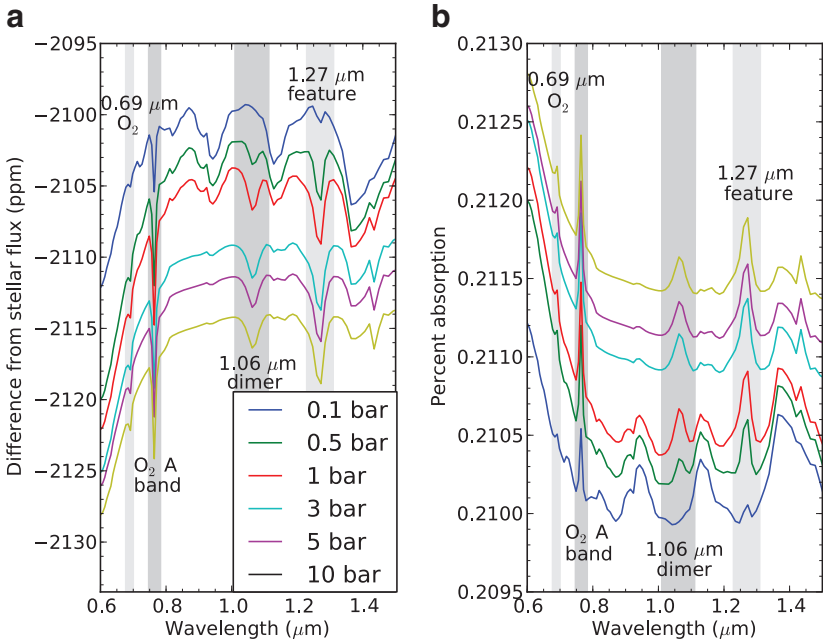

FIG. 7. Same as Fig. 4 but for 200% of the present-day level of O_2. The 1.06 μm dimer feature is very strong in every case except for the 0.1 bar atmosphere. (Color graphics available online at www.liebertonline.com/ast)

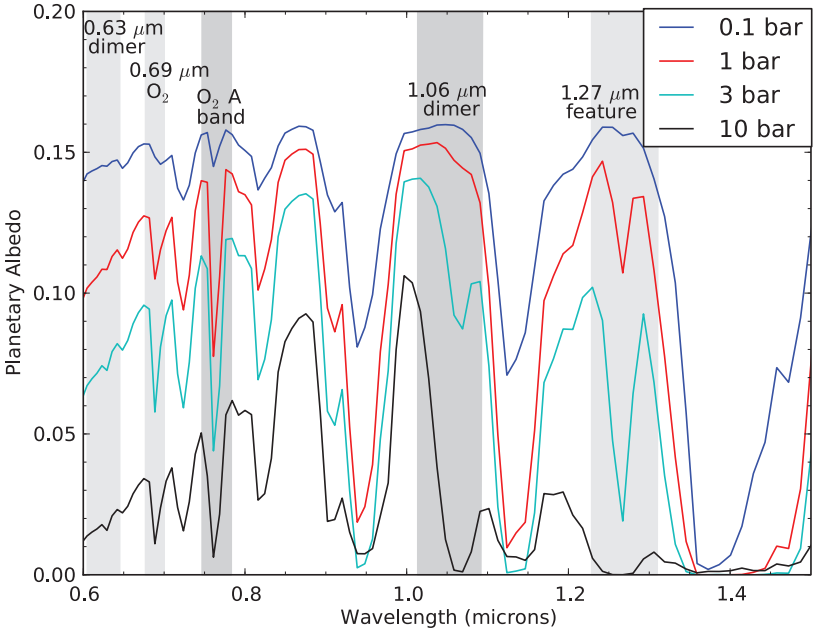

FIG. 8. Reflected spectra for Earth-like atmospheres with 100% PAL O_2 but with different total atmospheric pressures. In the reflected spectrum, there is no fundamental limit to which pressures can be probed in an atmosphere. Assuming a cloud-free case, it is possible to probe the surface layers of the atmosphere. The 1.06 μm dimer feature is fairly weak in the present-day Earth's atmosphere, but it is a very strong feature in atmospheres with greater pressures. The 1.27 μm feature is very strong in most of the spectra.

3.4. Sensitivity tests

To quantify the errors introduced by assuming the modern-day temperature profile, we generated spectra to test the sensitivity of our models to changes in the temperature profile and to changes in the water vapor profiles. We compared our 1.0 bar, 1.0×PAL O_2 spectra to a spectrum generated by using the same volume mixing ratio profiles but with an isothermal atmosphere at 250 K. We also compared our 1.0 bar, 1.0×PAL O_2 transit transmission spectrum to spectra generated with atmospheres with 0.1 and 10.0 times the H_2O levels. We perform a similar comparison for the 1.0 bar, 2.0×PAL O_2 reflected spectrum.

Figure 16 shows the sensitivity of the spectra to the temperature profile, with our Earth-like profile and an isothermal approximation profile compared. Both the transit transmission and reflected spectra show little sensitivity to the temperature profile. The 1.06 μm dimer band also shows little sensitivity to the temperature profile, despite the dependence of the dimer optical depth on the square of the temperature because the isothermal temperature profile approximates the average temperature of the troposphere, where the majority of dimer absorption occurs.

Figures 17, 18, and 19 show the results for the H_2O sensitivity tests. The O_2 A band equivalent widths and part-per-million flux differences are not strongly affected by changes in the H_2O profiles. However, changes in the H_2O mixing ratios affect the continuum flux in the wings of the 1.06 micron dimer feature, complicating measurements of the equivalent width of this feature. For the transit

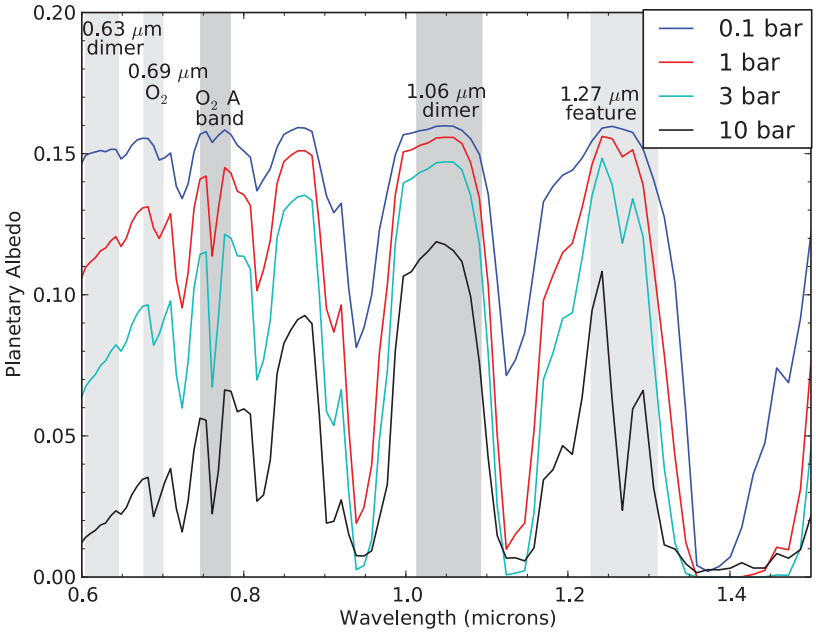

FIG. 9. Same as Fig. 8 but for an O_2 concentration of 10% PAL. For this amount of O_2, the 1.06 μm dimer feature is very weak. However, the 1.27 μm feature is still quite strong.

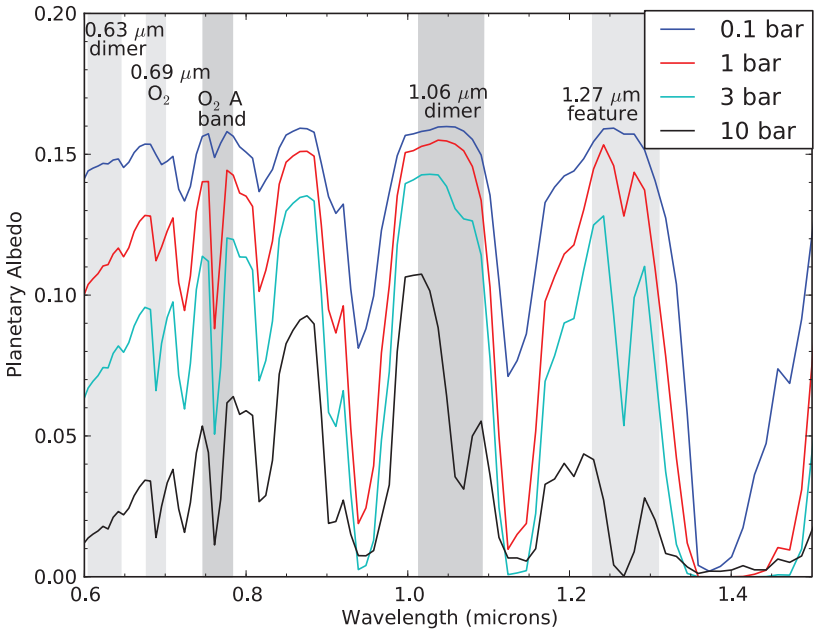

FIG. 10. Same as Fig. 8 but for an O_2 concentration of 50% PAL. The 1.06 μm dimer feature is strong at pressures ≥ 3 bar. (Color graphics available online at www.liebertonline.com/ast)

transmission spectra, the change in the total part-per-million flux difference (across the entire band) is less than 20% between the $0.1\times$ and $10.0\times H_2O$ cases. For the reflected spectra, the change in the equivalent width of the 1.06 μm dimer feature is less than 20%. For the reflected spectra, the equivalent widths can be much greater than that for the 1.0 bar, $2.0\times O_2$ case. For these greater equivalent widths, the effect of increasing or decreasing H_2O levels will diminish as the difference from the continuum flux (affected by H_2O), and the flux within the absorption band will increase.

3.5. Detectability of spectral features

Table 1 shows the SNRs for observations by JWST for the O_2 A band, 1.06 μm feature, and the 1.27 μm feature for the range of pressures and O_2 concentrations considered here for an Earth analogue at a distance of 5 pc. The SNR are calculated assuming that every transit of an Earth analogue orbiting an M5V star is observed over JWST's 5-year mission lifetime. In transit transmission, the O_2 A band SNRs are no greater than 1.1. The 1.06 μm dimer feature is detectable at a SNR of >3 for many of the $2.0\times$PAL O_2 cases. The 1.27 μm feature is the most detectable O_2 feature in this wavelength range, with SNRs greater than 5 for many of the $1.0\times$PAL O_2 cases and greater than 7 for many of the $2.0\times$PAL O_2 cases. JWST will not be able to detect O_2 species for Earth-like exoplanets in secondary eclipse in the visible and near-infrared, as shown by the secondary eclipse SNR levels. Even for the highest-pressure cases, the SNRs are no greater than ~ 0.2.

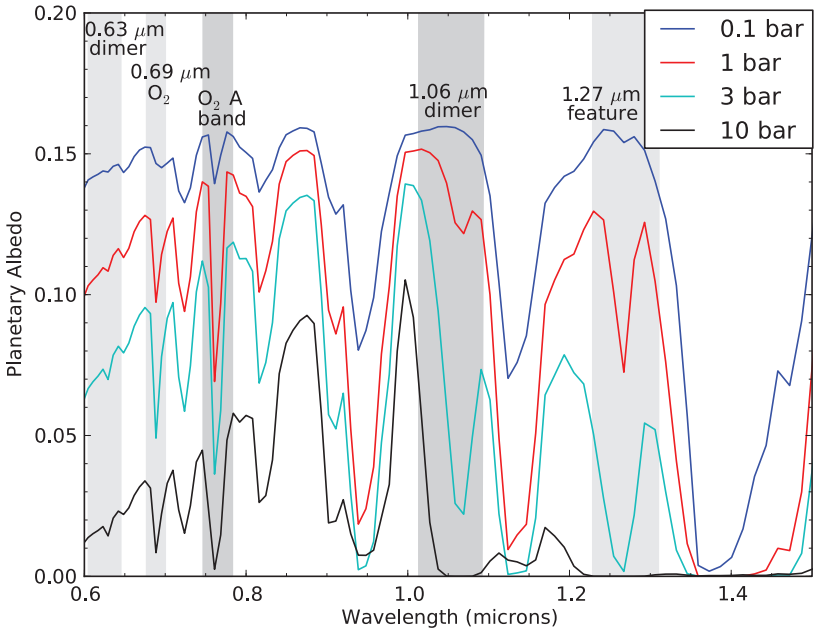

FIG. 11. Same as Fig. 8 but for an O_2 concentration of 200% PAL. The dimer features are much stronger with more O_2 in the atmosphere, as expected. (Color graphics available online at www.liebertonline.com/ast)

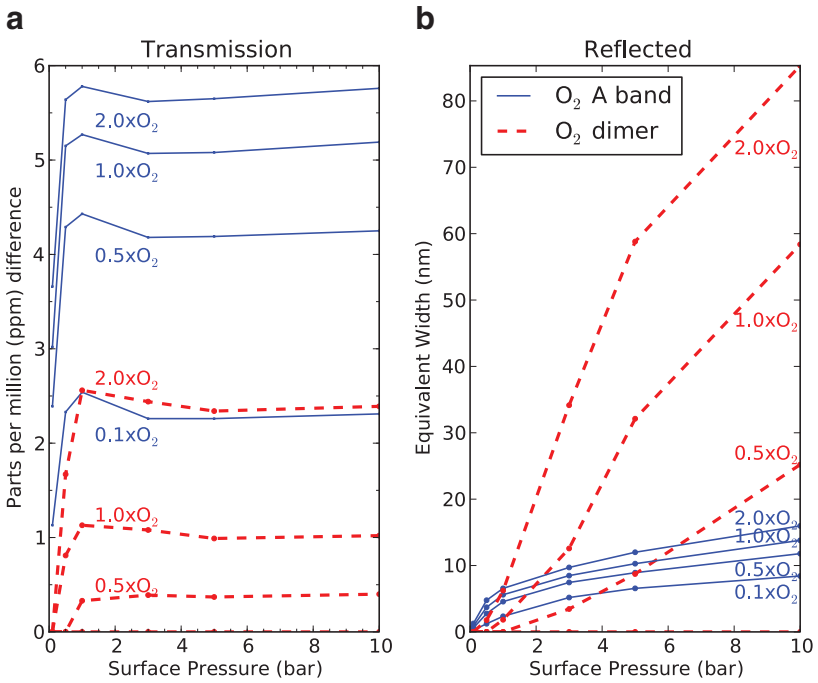

FIG. 12. (**a**) Flux differences (in ppm) for transit transmission spectra and (**b**) equivalent widths (in nm) for reflected spectra for the O_2 A band and the 1.06 μm dimer feature at various pressures and O_2 concentrations. In transmission, for the Earth-like planet orbiting an M5V star considered here, only the top 0.9 bar can be probed, meaning the dimer and A band equivalent widths are roughly constant with pressure above 1.0 bar for a given O_2 concentration. In comparison to the reflected spectra, the dimer equivalent widths are extremely sensitive to pressure. (Color graphics available online at www.liebertonline.com/ast)

Table 2 shows the SNRs necessary to detect and characterize the O_2 A band, 1.06 μm band, and the 1.27 μm feature for the range of pressures and O_2 concentrations considered here for the direct imaging reflected spectra at $R = 100$. The SNRs in Table 2 would be relevant to a direct imaging characterization mission. While these SNRs were calculated for an Earth analogue orbiting an M5V star, the results should be independent of stellar spectral type because we divided out the stellar flux in our calculations. The O_2 A band, 1.06 μm dimer feature, and 1.27 μm feature are detectable at an average SNR_D of 14, 9, and 14, respectively, for the cases when the features are strong enough to identify in the model spectra. The average required SNR_P to use the features for pressure estimation are 11, 31, and 34.

3.6. *Effect of spectral resolving power*

We examined the effect of spectral resolving power on the detectability of spectral features by generating transit transmission spectra for the 1.0 bar, 1.0 × PAL O_2 case with spectral resolving powers of 500, 200, 100, 80, 60, 40, 30, and 20. Figure 20 shows the spectra for each of these cases. We also measured the SNR of each feature at each resolving power. The SNRs were calculated assuming a noise profile

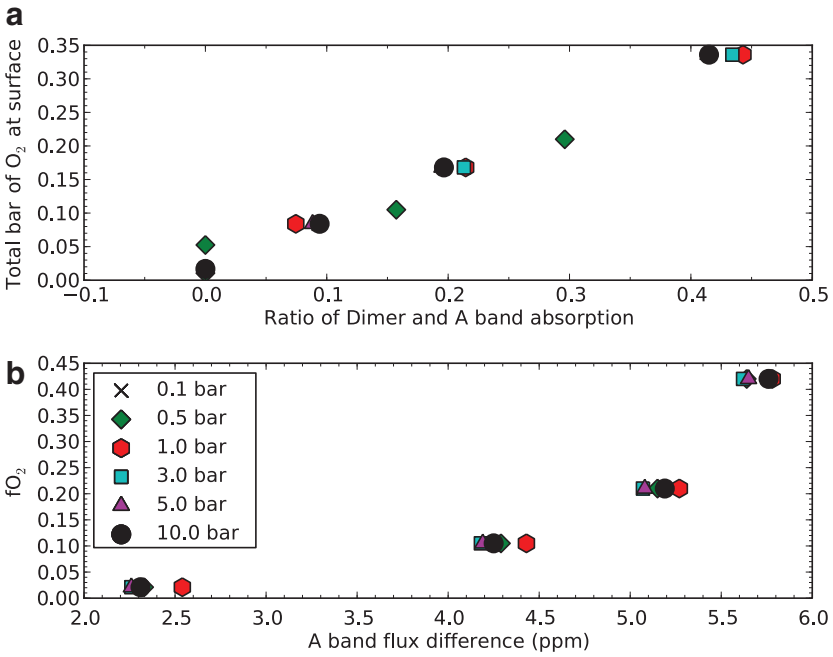

FIG. 13. This plot shows how one could determine a lower limit on the surface or cloud-top pressure using only a transmission spectrum. (**a**) O_2 partial pressure at maximum tangent pressure vs. the ratio of the dimer feature and O_2 A band flux difference ratio. The ratio can be used to determine the O_2 partial pressure. (**b**) fO_2 (or O_2 mixing ratio) vs. A band flux difference. The A band flux difference is roughly constant for a given O_2 mixing ratio. (Color graphics available online at www.liebertonline.com/ast)

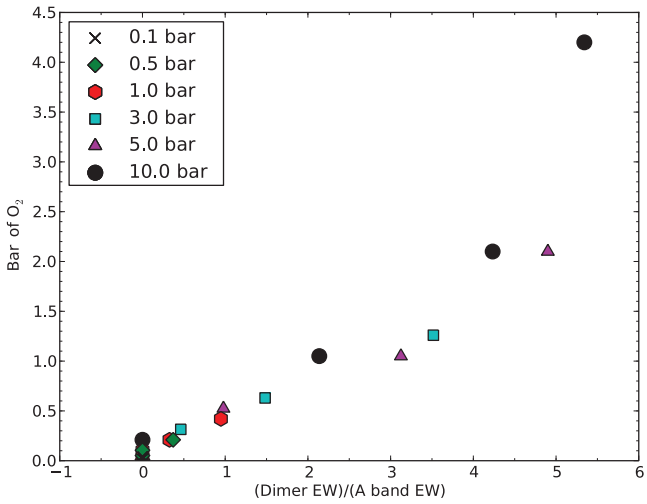

FIG. 14. Plot of total atmospheric O_2 vs. the ratio of the 1.06 μm dimer feature equivalent width (EW) to the O_2 A band equivalent width for the reflected spectrum. There is a trend between this ratio and the total amount of O_2. This could be used as a way to estimate the pressure if a transmission spectrum is not available. (Color graphics available online at www.liebertonline.com/ast)

equivalent to the JWST NIRSpec noise profile but with the noise level at each wavelength divided by $(100/R)^2$, so that the noise at each wavelength decreased as the resolving power decreased. Figure 21 shows how the total SNR in each absorption band changes with resolving power. In general, the SNRs drop off rapidly as resolving power decreases for $R<60$.

We also generated direct imaging reflected spectra for the 1.0 bar, 2.0×PAL O_2 case at resolving powers of 500, 200, 100, 80, 60, 40, 30, and 20, as shown in Fig. 22. Figures 23

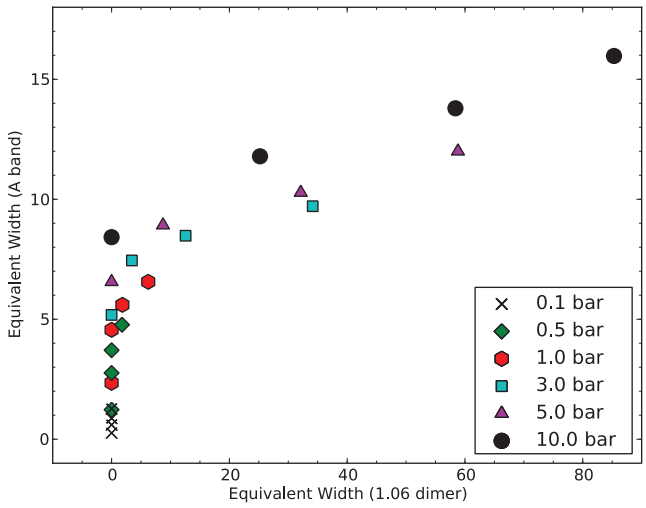

FIG. 15. Atmospheric pressure as a function of the dimer and A band equivalent widths in the reflected spectrum. It will be possible to set a lower bound on the pressure with only the O_2 A band equivalent width and the 1.06 μm dimer equivalent width. (Color graphics available online at www.liebertonline.com/ast)

and 24 show how the SNR for detection and precision vary with resolving power for the O_2 A band, 1.06 μm dimer feature, and the 1.27 μm feature. The SNR required to detect each feature increases as resolving power decreases. At $R=20$, the SNRs are not shown because no spectral features could be identified, and at $R=30$ only the O_2 A band was identified. The SNR required to quantify the flux at the center of each spectral feature decreases as resolving power decreases, because the lowest radiance level increases as the spectral resolving power decreases.

4. Discussion

The 1.06 μm dimer feature is prominent in transit transmission for atmospheres with ≥50% PAL O_2 and surface pressures ≥0.5 bar. It is a prominent feature in the reflected spectra for atmospheres with ≥50% PAL O_2 and surface pressure ≥3 bar. For the reflected spectra, the dimer feature equivalent width is highly dependent on surface pressure when compared to the O_2 A band; therefore the dimer feature can be used to constrain pressure. Here, we discuss how to do this for the cases investigated in this study.

4.1. Pressure measurement technique

Figure 12 confirms that dimer absorption features are more strongly dependent on pressure than monomer features. Therefore, dimer features can be combined with monomer features to determine pressure, even if the mixing ratio of the absorbing gas is not known. With only transit transmission spectroscopy, it is impossible to probe pressures over ~1 bar for the cases examined here, but it may be possible to constrain the O_2 mixing ratio and set a lower bound for pressure. In reflected spectra, it is possible to determine the surface partial pressure of O_2 and set a lower bound for pressure by using the 1.06 μm dimer feature as an on/off pressure gauge. With both a transit transmission spectrum and a reflected spectrum, it should be possible to determine total atmospheric surface pressure for an Earth-like exoplanet.

4.1.1. Transmission spectra pressure measurement. Transmission spectroscopy provides only a lower bound on the atmospheric pressure because refraction provides a fundamental limit to which pressures can be probed when using this technique. For the spectra presented here, a lower limit of ~1 bar can be set for the high-pressure atmospheres. For a given O_2 concentration, a unique estimate of the pressure can be retrieved from the ratio between the part-per-million flux differences of the 1.06 μm dimer feature and the O_2 A band. Figure 13a shows the relationship between this ratio and the total amount of O_2 above 0.9 bar, which is the highest pressure that can be probed in this particular case. There is a clear trend between this ratio and the amount of O_2 in the atmosphere. When combined with an O_2 mixing ratio, this relationship can provide a quantitative estimate of a lower level of the surface or cloud-top pressure.

The O_2 mixing ratio can be estimated from the flux difference of the O_2 A band in transmission. Figure 13b shows the relationship between the O_2 mixing ratio (which is constant throughout the atmosphere) and the O_2 A band flux difference. For pressure ≥0.1 bar, the O_2 flux difference is

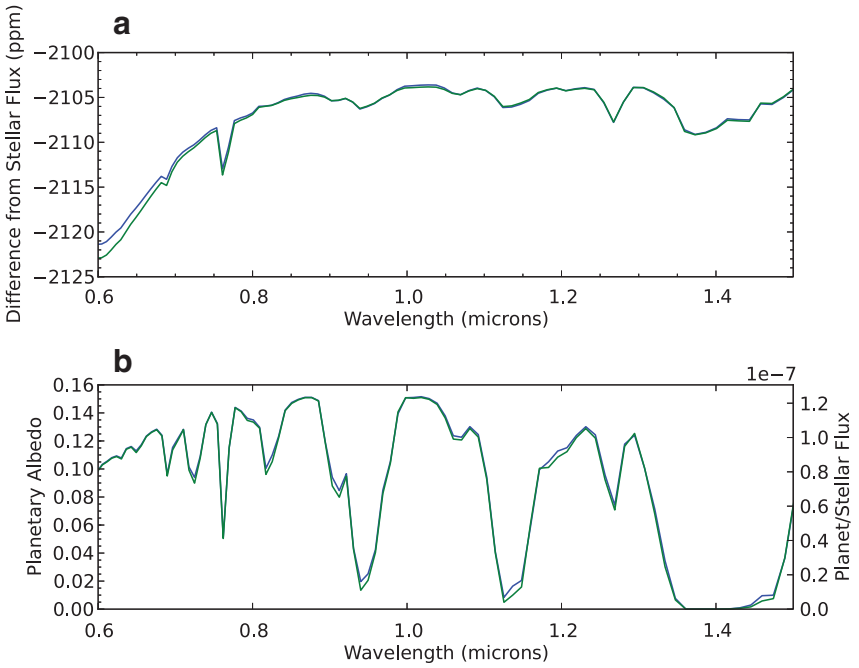

FIG. 16. (**a**) Transit transmission spectra for Earth (blue) and an isothermal atmosphere at 250 K with the same pressure-composition profiles (green). (**b**) Reflected spectra for an Earth analogue with 2.0×PAL O_2 (blue) and an isothermal atmosphere at 250 K with the same pressure-composition profiles (green). In both cases, the spectra for the calculated temperature-pressure profile and the isothermal profile are very similar, showing that the spectra are not strongly dependent on the temperature profile.

roughly constant for a given O_2 concentration, meaning that a measurement of the O_2 A band flux difference should correlate with the O_2 mixing ratio.

4.1.2. Reflected spectra pressure measurement. Reflected spectra alone can provide an estimate of the surface partial pressure of O_2 by examination of the ratio of the 1.06 μm dimer equivalent width and the O_2 A band equivalent width. Figure 14 shows the relationship between this ratio and the surface partial pressure of O_2. The strength of the 1.06 μm dimer feature could also be used as an on/off gauge to set a lower bound for pressure. Determining total atmospheric pressure with only a reflected spectrum is difficult due to degeneracies between the O_2 concentration and total atmospheric pressure, as shown in Fig. 15. For large equivalent widths of the dimer feature, the pressure will certainly be above 1 bar. However, it is difficult to differentiate between atmospheres with the same O_2 surface partial pressure. Nevertheless, it appears that it is possible to set a lower limit on pressure by measuring the 1.06 μm dimer feature equivalent width. For example, a 1.06 μm dimer feature equivalent width greater than $\sim$10 nm would imply a surface pressure $>$1 bar.

4.1.3. Pressure measurement with both transit transmission and reflected spectra. If both a transit transmission spectrum and a reflected spectrum are available, it should be possible to directly measure the total atmospheric surface

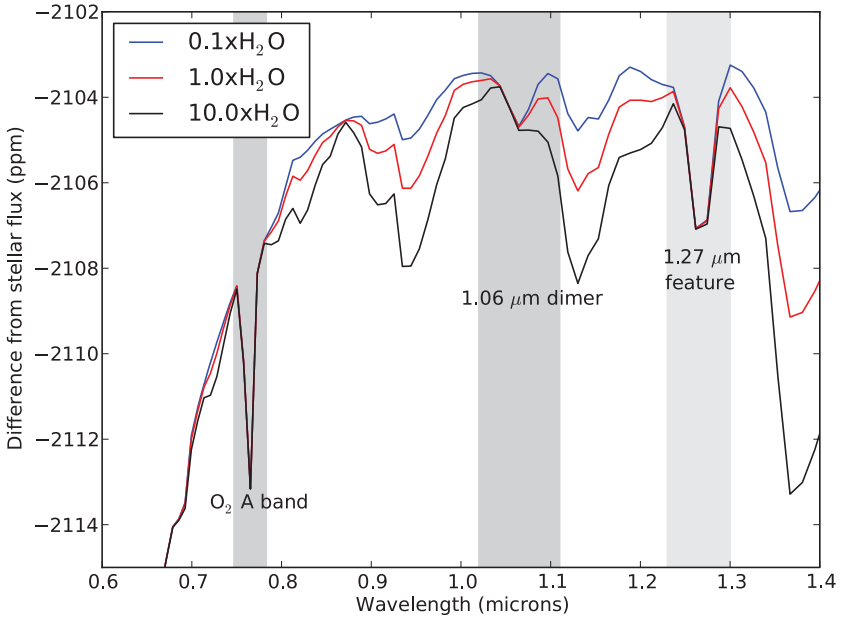

FIG. 17. Transit transmission spectra of a 1.0 bar, 1.0×PAL O_2 Earth analogue with H_2O concentrations varying from 0.1×to 10.0×PAL H_2O. While H_2O absorbs near the wings of the O_2 A band, the part-per-million flux difference and the SNR do not change greatly as the H_2O concentration changes. The continuum near the 1.06 μm dimer feature is strongly affected by the increases in H_2O. However, the magnitude of the change in the part-per-million flux difference over the entire band and the SNR is less than 20% when comparing the 1.0×PAL H_2O case to either the 0.1×or 10.0×H_2O cases.

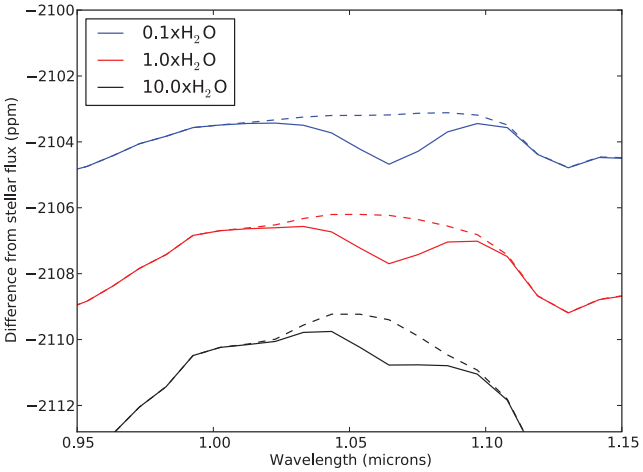

FIG. 18. The 1.06 μm dimer feature in transit transmission with different amounts of H_2O. The spectra have been artificially offset for ease of viewing. The dashed lines are spectra that do not include any O_2 dimer absorption and are included to help show the continuum flux level. The total part-per-million flux difference and SNR for the dimer band vary by less than 20% with respect to the $1.0\times H_2O$ case. (Color graphics available online at www.liebertonline.com/ast)

pressure in the absence of clouds. Transit transmission spectroscopy can provide an estimate of the O_2 mixing ratio as described previously. A reflected spectrum can theoretically probe to the reflecting surface and therefore can be used to constrain the O_2 partial pressure at the surface. By combining the O_2 mixing ratio and O_2 partial pressure, we

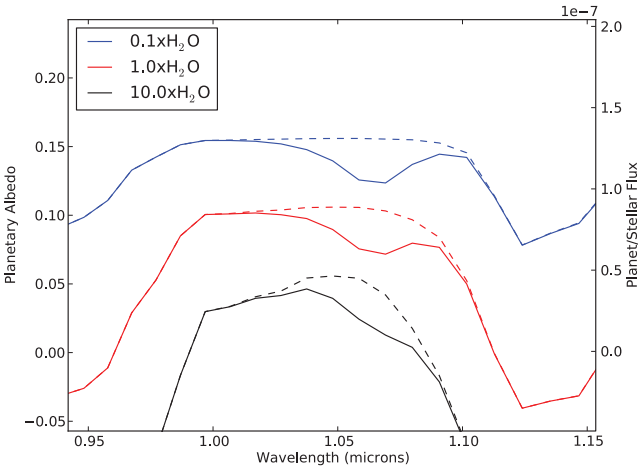

FIG. 19. The 1.06 μm dimer feature in the direct beam reflected spectra with varying amounts of H_2O for an Earth analogue with a 1.0 bar, $2.0\times$PAL O_2 atmosphere. There is an artificial offset for ease of viewing, and the dashed lines are spectra that do not include any O_2 dimer absorption. As in transit transmission, the SNR of the dimer feature varies by less than 20% with respect to the $1.0\times H_2O$ case. Additionally, the SNRs for higher-pressure cases should be less affected by changes in H_2O concentrations because of greater absorption within the dimer band. (Color graphics available online at www.liebertonline.com/ast)

can determine the total pressure at the reflecting surface, which could either be a reflective cloud layer or the physical surface of the planet.

4.2. Relevance to planet characterization

The methods described here could be used in the near future by the JWST NIRSpec instrument, which will potentially be able to characterize transiting planets between 0.6 and 5.0 μm. The O_2 A band will likely not be detectable for a nearby Earth analogue with JWST. Although this feature is strong in the spectrum, the sensitivity of NIRSpec is poor at shorter wavelengths. The 1.06 μm dimer feature is detectable at the 3σ level in transit transmission for cases with $2.0\times$PAL O_2 and high surface pressures. Thus, the detection of the 1.06 μm dimer feature would imply a surface or cloud-top pressure greater than or equal to 1.0 bar. For cases in which the 1.06 μm dimer feature is not detectable, the 1.27 μm feature could be used to constrain the pressure. This feature is not as strongly dependent on pressure as the 1.06 μm dimer feature, but it is more detectable in all cases explored here.

Terrestrial Planet Finder or a similar direct imaging mission will be required to characterize the reflected spectra of nearby Earth analogues in the visible and near-infrared. The SNR values for secondary eclipse applicable to JWST are all less than 1, so JWST will not be able to characterize the reflected spectra of Earth analogues in secondary eclipse. Table 2 shows the necessary SNRs to detect and characterize spectral features for a direct imaging planet characterization mission. While the SNRs were calculated for an Earth analogue orbiting an M5V star, the results should be largely independent of spectral type because we have divided the reflected flux by the stellar flux in our calculations. The required SNR values suggest that a SNR of >10 would be necessary to detect and quantify the O_2 A band, 1.06 μm dimer feature, and 1.27 μm feature for a true Earth analogue. However, because continuum brightness changes with pressure, a different SNR criteria would be necessary for higher-pressure atmospheres. For example, the continuum brightness near the O_2 A band is 3 times lower for the 10.0 bar cases than it is for the 0.1 bar cases. For most cases, a SNR of >7 would likely be sufficient to set a lower limit on the surface pressure when using the 1.06 μm dimer feature.

Clouds and aerosols will also affect the detectability of absorption features. In transit transmission, clouds can effectively mask the highest pressures of the atmospheres at which dimer absorption is most prominent. However, in partially cloudy atmospheres, some of the paths will probe pressures as high as the maximum tangent pressure; thus the planetary transmission spectrum could show evidence of dimer absorption. Furthermore, absorption in the 1.27 μm dimer band can be detected with SNR >1 in even some 0.1 bar cases, meaning that there could be a detectable dimer absorption signal for even a completely cloud-covered planet if the cloud deck pressure was ≥ 0.1 bar. For reflected spectra, clouds will truncate paths before they reach the surface and limit the dimer absorption for those paths. However, for partially cloudy atmospheres, dimer absorption could be detectable in the paths that do reach the surface. Additionally, because cloud albedos are typically

Table 1. Signal-to-Noise Ratios for the O_2 A Band, the 1.06 μm Dimer Feature, and the 1.27 μm Feature for All the Cases Considered in Both Transit Transmission and Secondary Eclipse

Pressure	fO_2	*Transit transmission*			*Secondary eclipse*		
Bar	*PAL*	*O_2 A band*	*O_2-O_2 1.06 μm*	*O_2 1.27 μm*	*O_2 A band*	*O_2-O_2 1.06 μm*	*O_2 1.27 μm*
0.1	0.1	0.2	0.0	0.0	5.2e-04	0.0e+00	2.7e-03
0.1	0.5	0.5	0.0	0.9	1.2e-03	0.0e+00	3.4e-03
0.1	1.0	0.6	0.0	1.2	1.7e-03	0.0e+00	4.2e-03
0.1	2.0	0.8	0.0	1.5	2.4e-03	0.0e+00	5.5e-03
0.5	0.1	0.5	0.0	1.1	2.3e-03	0.0e+00	5.5e-03
0.5	0.5	0.8	0.0	2.5	5.0e-03	0.0e+00	1.2e-02
0.5	1.0	1.1	1.2	3.7	6.7e-03	0.0e+00	1.8e-02
0.5	2.0	1.1	2.3	5.1	8.5e-03	1.2e-02	2.7e-02
1.0	0.1	0.5	0.0	1.6	4.1e-03	0.0e+00	9.5e-03
1.0	0.5	0.8	0.5	3.9	7.8e-03	0.0e+00	2.6e-02
1.0	1.0	1.1	1.5	5.2	9.4e-03	1.3e-02	3.9e-02
1.0	2.0	1.1	3.4	7.5	1.1e-02	3.5e-02	6.3e-02
3.0	0.1	0.5	0.0	1.2	7.3e-03	0.0e+00	3.2e-02
3.0	0.5	0.8	0.6	3.5	1.0e-02	2.1e-02	8.4e-02
3.0	1.0	1.1	1.5	5.0	1.1e-02	6.2e-02	9.9e-02
3.0	2.0	1.1	3.5	7.2	1.2e-02	1.5e-01	1.2e-01
5.0	0.1	0.5	0.0	1.1	7.5e-03	0.0e+00	5.8e-02
5.0	0.5	0.8	0.6	3.3	9.6e-03	4.3e-02	1.1e-01
5.0	1.0	1.1	1.4	4.9	1.1e-02	1.2e-01	9.4e-02
5.0	2.0	1.1	3.3	7.2	1.2e-02	2.1e-01	1.1e-01
10.0	0.1	0.5	0.0	1.1	5.9e-03	0.0e+00	9.2e-02
10.0	0.5	0.8	0.7	3.4	7.8e-03	9.3e-02	6.1e-02
10.0	1.0	1.1	1.4	5.0	8.6e-03	1.7e-01	6.1e-02
10.0	2.0	1.1	3.4	7.4	9.0e-03	2.1e-01	5.0e-02

The calculations were done for an Earth analogue orbiting an M5V star at a distance of 5 pc. The total integration time was assumed to be 10^6 s, equal to the total amount of time spent in transit for this case over JWST's 5-year mission lifetime. The 1.06 μm dimer feature and the 1.27 μm feature could be detectable, allowing a lower limit for atmospheric pressure to be set.

greater than surface albedos, the presence of clouds will increase the continuum brightness levels and the brightness in the center of absorption bands. The increase in brightness has been shown to decrease the required SNR to detect and characterize O_2 monomer absorption in cloudy atmospheres when compared to cloud-free cases (Evans *et al.,* 2011), though the effect of cloud albedo on the detectability of dimer absorption features has not been heretofore examined. Therefore, while clouds will impact the detectability of dimer features, using dimers to determine pressure and as biosignatures may still be feasible for cloudy atmospheres.

4.3. Detectability at different resolving powers

Figure 21 shows the SNRs for spectral features at varying resolving powers for transit transmission spectra of a 1.0 bar, 1.0×PAL O_2 atmosphere. The SNRs for each band are greatest at the highest resolving powers and then gradually decrease until $R \sim 60$ or 80, at which the SNRs decrease strongly. This dramatic decrease with resolving power occurs because, at the lowest resolving powers, the absorption bands are indistinguishable from the continuum. Additionally, the highest flux levels in the continuum cannot be resolved at lower spectral resolving powers, decreasing the total signal. This effect can be seen most easily for the spectra with $R = 20$, in which no absorption features can be identified.

Figures 23 and 24 show the SNRs for the direct imaging reflected spectra. In contrast to Fig. 21, these two figures show the required SNR to detect and characterize an absorption band, not the SNR that could be obtained with JWST. The required SNR to detect spectral features increases as resolving power decreases. However, this effect would be mitigated because the expected noise at each wavelength should decrease as resolving power decreases. The SNR required to quantify each absorption band decreases as resolving power decreases because the lowest radiance level increases. At $R < 40$, however, spectral features are very difficult to identify, making these resolving powers unsuitable for detecting and characterizing O_2-related absorption features.

4.4. O_2 dimer biosignatures

In addition to their utility as pressure probes, the 1.06 μm dimer feature and 1.27 μm feature could potentially be detectable biosignatures for nearby Earth-like planets. The O_2 A band has long been considered the most viable O_2 biosignature, but it is unlikely to be the most detectable biosignature for an Earth-like planet in transit transmission. As initially described by Pallé *et al.* (2009), lunar eclipse observations show that the 1.06 and 1.27 μm dimer features are more detectable than O_2 monomer features like the A band, which is corroborated by our model spectra and detectability calculations. The 1.27 μm O_2 feature has been examined as a potential biosignature for ground-based telescopes by Kawahara *et al.* (2012), but to our knowledge detectability studies of neither the 1.06 μm dimer feature nor the 1.27 μm

TABLE 2. SIGNAL-TO-NOISE RATIOS FOR DETECTION (SNR_D) AND TO OBTAIN PRECISION OF 3σ IN THE CENTER OF THE BAND (SNR_P) FOR THE O_2 A BAND, THE 1.06 μm DIMER FEATURE, AND THE 1.27 μm FEATURE AT PRESSURES RANGING FROM 0.1 TO 10.0 BAR AND O_2 CONCENTRATIONS RANGING FROM 0.1 TO 2.0 TIMES PAL O_2 FOR DIRECT IMAGING REFLECTED SPECTRA

Pressure	fO_2	*O_2 A band*		*1.06 μm dimer*		*1.27 μm feature*	
Bar	*PAL*	*SNR_D*	*SNR_P*	*SNR_D*	*SNR_P*	*SNR_D*	*SNR_P*
0.1	0.1	>100	3.1	—	—	—	—
0.1	0.5	50.0	3.2	—	—	>100	3.0
0.1	1.0	35.0	5.4	—	—	>100	5.1
0.1	2.0	24.4	3.4	—	—	89.8	3.1
0.5	0.1	25.1	3.4	—	—	>100	3.1
0.5	0.5	11.4	3.9	—	—	38.8	3.2
0.5	1.0	8.6	7.3	—	—	23.8	5.6
0.5	2.0	6.8	5.0	30.9	3.2	14.3	3.7
1.0	0.1	13.4	3.8	—	—	62.0	3.1
1.0	0.5	7.1	4.8	—	—	16.4	3.6
1.0	1.0	5.8	9.1	29.0	5.4	9.9	6.9
1.0	2.0	5.0	6.1	9.6	3.7	5.9	5.4
3.0	0.1	6.2	5.3	—	—	12.8	3.8
3.0	0.5	4.4	6.9	16.5	3.4	4.3	7.2
3.0	1.0	3.9	13.2	4.9	8.1	2.9	26.7
3.0	2.0	3.5	9.4	1.9	18.9	1.7	>100
5.0	0.1	5.0	6.3	—	—	6.5	5.0
5.0	0.5	3.8	8.6	6.8	4.1	2.7	20.9
5.0	1.0	3.4	17.7	2.3	18.1	1.9	>100
5.0	2.0	3.0	15.2	1.3	>100	1.3	>100
10.0	0.1	4.1	8.1	—	—	3.0	13.7
10.0	0.5	3.0	15.2	2.3	10.4	1.8	>100
10.0	1.0	2.7	44.9	1.4	>100	1.2	>100
10.0	2.0	2.4	61.6	1.0	>100	1.0	>100

feature have been undertaken for JWST. Our results show that the 1.27 μm feature would be detectable with a SNR of 5 for a cloud-free Earth analogue at 5 pc. Therefore, we conclude that O_2 features, especially the 1.06 μm dimer feature and the 1.27 μm feature, could be detectable biosignatures for oxygenic photosynthesis with JWST.

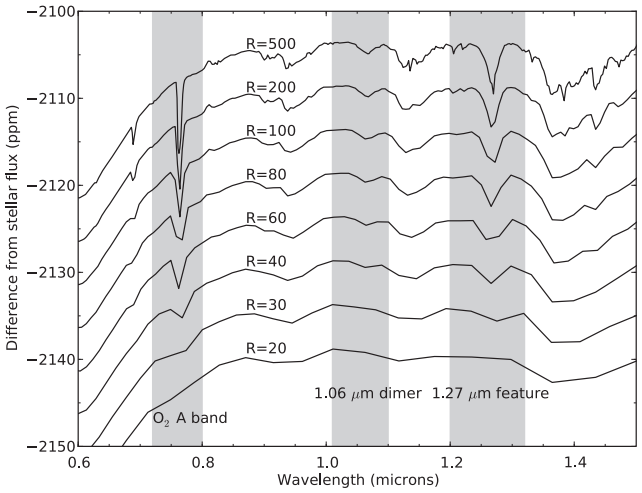

FIG. 20. Transit transmission spectra for the 1.0 bar, 1.0×PAL O_2 case at various spectral resolving powers. The wavelengths for the O_2 A band, the 1.06 μm dimer band, and the 1.27 μm band are highlighted. An artificial offset has been added to the spectra for ease of viewing. At the lowest resolving powers, it is difficult to identify spectral features.

4.5. Challenges to observations

Clouds and aerosols will make estimating pressure by using dimer features more difficult. A direct imaging observation of a partially cloud-covered planet will be able to probe to the surface for a fraction of the paths, such that the dimer feature will be weaker than for a cloud-free planet. Cloud and aerosol extinction can also be wavelength-dependent, which may complicate using equivalent widths or part-per-million flux differences to determine pressure. Nevertheless, dimer features can still provide a lower bound for pressure if clouds and aerosols cannot be explicitly included in the retrieval method.

Higher H_2O or CO_2 abundances in an atmosphere could also make this method more challenging. Higher H_2O abundances will make it more difficult to define a continuum for the 1.06 μm dimer feature, as shown in Figs. 18 and 19. However, as discussed in Section 3.4, the magnitude of this error should typically be less than 20% for most cases in which the 1.06 μm dimer feature could be detectable. CO_2 has an absorption feature near 1.06 μm (Segura *et al.,* 2007), which could make using the 1.06 μm dimer feature difficult. This could be overcome by modeling out absorption from H_2O and CO_2 or by using other dimer features to supplement information from the 1.06 μm dimer feature, such as the 1.27 μm dimer feature.

Lastly, not knowing the mixing ratio of O_2 will make estimating pressure difficult when only a reflected spectrum is available. This is similar to the problem in using the absorption widths of rotation-vibration features to constrain pressure. However, the 1.06 μm dimer feature is more

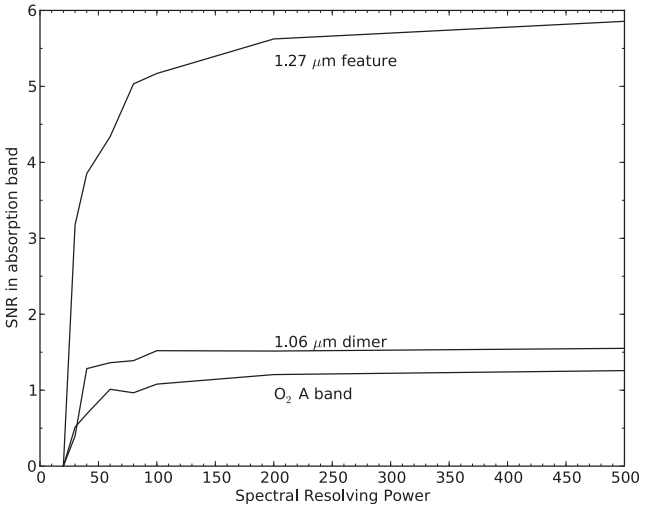

FIG. 21. Signal-to-noise ratios of absorption features for the spectra shown in Fig. 20. The SNRs decrease as resolving power decreases because the absorption bands can no longer be resolved from the continuum. For $R = 30$ and $R = 20$ it is very difficult to identify any of the O_2 spectral features.

sensitive to pressure than a monomer feature and therefore can provide a better estimate of pressure than a monomer feature alone. Furthermore, monomer features cannot be used as an on/off pressure gauge, while dimer features can.

5. Conclusions

Spectrally resolved observations of O_2 dimer absorption can be combined with observations of the absorption by O_2 vibration-rotation bands to provide independent constraints

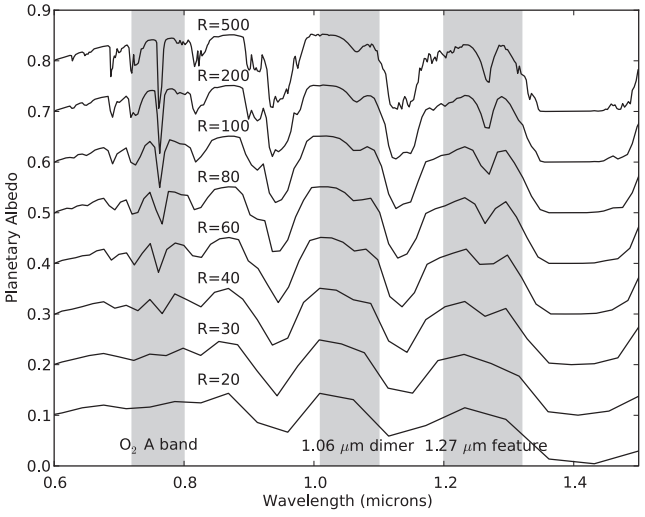

FIG. 22. Direct imaging reflected spectra generated at spectral resolving powers from 500 to 20. The *y* axis is the planetary albedo with an arbitrary offset added for ease of viewing. The O_2 A band, 1.06 μm dimer feature, and 1.27 μm feature are highlighted. At resolving powers of $R = 30$ and $R = 20$ it is difficult to identify any O_2 absorption features.

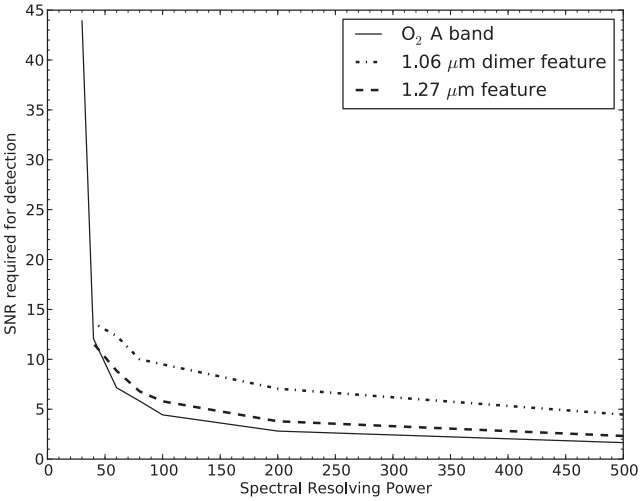

FIG. 23. Signal-to-noise ratios needed to detect the O_2 A band, 1.06 μm dimer feature, and the 1.27 μm feature for direct imaging reflected spectra. As resolving power decreases, the required SNR to detect each feature increases because the continuum level decreases, resulting in a lower overall signal in the absorption band. Furthermore, at the lowest resolutions, the absorption bands cannot be resolved. Thus, this decreases the measurable signal even more, leading to an increase in the required SNR.

on the O_2 concentration and the surface or cloud-top pressure in oxygenated atmospheres for planets around M dwarfs, and with low levels of CO_2. Even if a precise estimate for the pressure is not possible, the presence of dimer absorption is indicative of pressures greater than ~ 0.5 bar

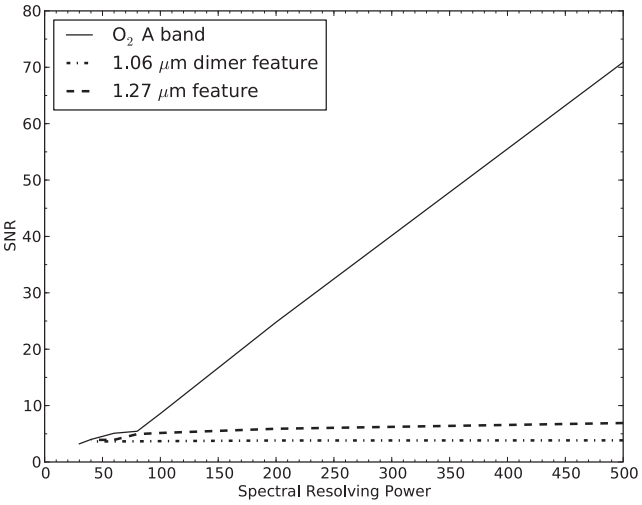

FIG. 24. Signal-to-noise ratios required to quantify the flux within 3σ in the center of the absorption band (defined as the lowest flux level) for the O_2 A band, 1.06 μm dimer feature, and the 1.27 μm feature. The SNR required for this level of precision decreases as resolving power decreases because the flux is averaged over fewer wavelength bins, leading to an increase in the lowest flux. This decrease in required resolving power occurs for all three absorption features, though the trend is most apparent for the O_2 A band, as it has the narrowest spectral shape of the three features considered here.

in transmission spectroscopy and greater than ~ 1 bar in reflected spectra.

We have shown that this method is feasible in the absence of clouds for oxygenated atmospheres. For transmission spectroscopy, this method can be used to estimate the surface or cloud-top pressure for O_2 concentrations $\geq 100\%$ PAL and for pressures > 0.5 bar. For reflected spectra, this method will work if the O_2 partial pressure at the surface is > 0.3 bar. Clouds will reduce the absorption strength of dimer features by limiting the paths that can probe the highest pressures in transit transmission and by truncating paths before they reach the surface in the reflected spectra.

The James Webb Space Telescope may be able to detect the 1.06 μm dimer feature and the 1.27 μm O_2 feature for an Earth analogue orbiting an M dwarf in transit transmission. Thus, while not all the techniques described here will be applicable to JWST observations, a lower bound on pressure could be set for an exoplanet by using an O_2 dimer feature. Furthermore, we showed that a direct imaging mission operating in the visible and near-infrared like Terrestrial Planet Finder would require a spectral resolving power of $R > 40$ and preferably higher. At $R = 100$, a SNR of > 10 would be required not only to detect O_2-related absorption features but also to provide an estimate of an exoplanet's atmospheric pressure.

Acknowledgments

We thank Drake Deming for helpful discussions on the detectability calculations and the two anonymous reviewers for their thorough and helpful reviews that greatly improved the paper.

This work was performed by the NASA Astrobiology Institute's Virtual Planetary Laboratory, supported by the National Aeronautics and Space Administration through the NASA Astrobiology Institute under Cooperative Agreement solicitation NNH05ZDA001C. This work has also been supported by a generous fellowship from the ARCS Seattle chapter and funding from the Astrobiology Program at the University of Washington under an NSF IGERT award.

Some of the work described here was conducted at the Jet Propulsion Laboratory, California Institute of Technology, under contract with NASA.

This research has made use of NASA's Astrophysics Data System.

Author Disclosure Statement

No competing financial interests exist.

Abbreviations

JWST, James Webb Space Telescope; NIRSpec, Near-Infrared Spectrograph; PAL, present atmospheric level; SMART, Spectral Mapping Atmospheric Radiative Transfer; SNR, signal-to-noise ratio.

References

Acarreta, J.R., de Haan, J.F., and Stammes, P. (2004) Cloud pressure retrieval using the O_2-O_2 absorption band at 477 nm. *J Geophys Res (Atmospheres)* 109:5204–5214.

Auer, L.H. and Standish, E.M. (2000) Astronomical refraction: computational method for all zenith angles. *Astron J* 119: 2472–2474.

Baldridge, A.M., Hook, S.J., Grove, C.I., and Rivera, G. (2009) The ASTER Spectral Library version 2.0. *Remote Sens Environ* 113:711–715.

Barton, I.J. and Scott, J.C. (1986) Remote measurement of surface pressure using absorption in the oxygen A-band. *Appl Opt* 25:3502–3507.

Bean, J.L., Miller-Ricci Kempton, E., and Homeier, D. (2010) A ground-based transmission spectrum of the super-Earth exoplanet GJ 1214b. *Nature* 468:669–672.

Belu, A.R., Selsis, F., Morales, J.-C., Ribas, I., Cossou, C., and Rauer, H. (2011) Primary and secondary eclipse spectroscopy with JWST: exploring the exoplanet parameter space. *Astron Astrophys* 525:A83–A97.

Brown, T.M. (2001) Transmission spectra as diagnostics of extrasolar giant planet atmospheres. *Astrophys J* 553:1006–1026.

Carey, S., Ingalls, J., Hora, J., Surace, J., Glaccum, W., Lowrance, P., Krick, J., Cole, D., Laine, S., Engelke, C., Price, S., Bohlin, R., and Gordon, K. (2012) Absolute photometric calibration of IRAC: lessons learned using nine years of flight data. *Proc SPIE* 8442, doi:10.1117/12.927183.

Catling, D.C., Claire, M.W., Zahnle, K.J., Quinn, R.C., Clark, B.C., Hecht, M.H., and Kounaves, S. (2010) Atmospheric origins of perchlorate on Mars and in the Atacama. *J Geophys Res (Planets)* 115, doi:10.1029/2009JE003425.

Chamberlain, S., Bailey, J., Crisp, D., and Meadows, V. (2013) Ground-based near-infrared observations of water vapour in the Venus troposphere. *Icarus* 222:364–378.

Chamberlain, S.A., Bailey, J.A., and Crisp, D. (2006) Mapping martian atmospheric pressure with ground-based near infrared spectroscopy. *Publications of the Astronomical Society of Australia* 23:119–124.

Charbonneau, D., Brown, T.M., Noyes, R.W., and Gilliland, R.L. (2002) Detection of an extrasolar planet atmosphere. *Astrophys J* 568:377–384.

Clark, R.N., Swayze, G.A., Wise, R., Livo, E., Hoefen, T., Kokaly, R., and Sutley, S.J., (2007) USGS Digital Spectral Library splib06a. Digital Data Series 231, U.S. Geological Survey, Reston, VA.

Crisp, D. (1997) Absorption of sunlight by water vapor in cloudy conditions: a partial explanation for the cloud absorption anomaly. *Geophys Res Lett* 24:571–574.

Crisp, D., Fisher, B.M., O'Dell, C., Frankenberg, C., Basilio, R., Bösch, H., Brown, L.R., Castano, R., Connor, B., Deutscher, N.M., Eldering, A., Griffith, D., Gunson, M., Kuze, A., Mandrake, L., McDuffie, J., Messerschmidt, J., Miller, C.E., Morino, I., Natraj, V., Notholt, J., O'Brien, D.M., Oyafuso, F., Polonsky, I., Robinson, J., Salawitch, R., Sherlock, V., Smyth, M., Suto, H., Taylor, T.E., Thompson, D.R., Wennberg, P.O., Wunch, D., and Yung, Y.L. (2012) The ACOS CO_2 retrieval algorithm—part II: global X_{CO_2} data characterization. *Atmospheric Measurement Techniques* 5:687–707.

Crow, C.A., McFadden, L.A., Robinson, T., Meadows, V.S., Livengood, T.A., Hewagama, T., Barry, R.K., Deming, L.D., Lisse, C.M., and Wellnitz, D. (2011) Views from EPOXI: colors in our solar system as an analog for extrasolar planets. *Astrophys J* 729:130–139.

Deming, D., Seager, S., Winn, J., Miller-Ricci, E., Clampin, M., Lindler, D., Greene, T., Charbonneau, D., Laughlin, G., Ricker, G., Latham, D., and Ennico, K. (2009) Discovery and characterization of transiting super Earths using an all-sky

transit survey and follow-up by the James Webb Space Telescope. *Publ Astron Soc Pac* 121:952–967.

Deming, D., Wilkins, A., McCullough, P., Burrows, A., Fortney, J.J., Agol, E., Dobbs-Dixon, I., Madhusudhan, N., Crouzet, N., Desert, J.M., Gilliland, R.L., Haynes, K., Knutson, H.A., Line, M., Magic, Z., Mandell, A.M., Ranjan, S., Charbonneau, D., Clampin, M., Seager, S., and Showman, A.P. (2013) Infrared transmission spectroscopy of the exoplanets HD 209458b and XO-1b using the Wide Field Camera-3 on the Hubble Space Telescope. *Astrophys J* 774: 95–111.

Domagal-Goldman, S.D., Meadows, V.S., Claire, M.W., and Kasting, J.F. (2011) Using biogenic sulfur gases as remotely detectable biosignatures on anoxic planets. *Astrobiology* 11: 419–441.

Evans, N., Meadows, V.S., and Domagal-Goldman, S.D. (2011) Exploring the detectability of terrestrial exoplanet characteristics [presentation number 343.09]. In *Bulletin of the American Astronomical Society,* Vol. 43, AAS Meeting #217.

Forget, F., Spiga, A., Dolla, B., Vinatier, S., Melchiorri, R., Drossart, P., Gendrin, A., Bibring, J.-P., Langevin, Y., and Gondet, B. (2007) Remote sensing of surface pressure on Mars with the Mars Express/OMEGA spectrometer: 1. Retrieval method. *J Geophys Res (Planets)* 112:8–25.

García Muñoz, A., Zapatero Osorio, M.R., Barrena, R., Montañés-Rodríguez, P., Martín, E.L., and Pallé, E. (2012) Glancing views of the Earth: from a lunar eclipse to an exoplanetary transit. *Astrophys J* 755:103–112.

Gardner, J.P., Mather, J.C., Clampin, M., Doyon, R., Greenhouse, M.A., Hammel, H.B., Hutchings, J.B., Jakobsen, P., Lilly, S.J., Long, K.S., Lunine, J.I., McCaughrean, M.J., Mountain, M., Nella, J., Rieke, G.H., Rieke, M.J., Rix, H.-W., Smith, E.P., Sonneborn, G., Stiavelli, M., Stockman, H.S., Windhorst, R.A., and Wright, G.S. (2006) The James Webb Space Telescope. *Space Sci Rev* 123:485–606.

Gray, L.D. (1966) Transmission of the atmosphere of Mars in the region of 2 μm. *Icarus* 5:390–398.

Greenblatt, G.D., Orlando, J.J., Burkholder, J.B., and Ravishankara, A.R. (1990) Absorption measurements of oxygen between 330 and 1140 nm. *J Geophys Res* 95:18577–18582.

Hauschildt, P.H., Allard, F., and Baron, E. (1999) The NextGen model atmosphere grid for $3000 \leq T_{\rm eff} \leq 10{,}000$ K. *Astrophys J* 512:377–385.

Hubbard, W.B., Fortney, J.J., Lunine, J.I., Burrows, A., Sudarsky, D., and Pinto, P. (2001) Theory of extrasolar giant planet transits. *Astrophys J* 560:413–419.

Ignatiev, N.I., Titov, D.V., Piccioni, G., Drossart, P., Markiewicz, W.J., Cottini, V., Roatsch, T., Almeida, M., and Manoel, N. (2009) Altimetry of the Venus cloud tops from the Venus Express observations. *J Geophys Res (Planets)* 114, doi:10.1029/2008JE003320.

Kaltenegger, L. and Traub, W.A. (2009) Transits of Earth-like planets. *Astrophys J* 698:519–527.

Kaplan, L.D., Munch, G., and Spinrad, H. (1964) An analysis of the spectrum of Mars. *Astrophys J* 139:1–16.

Kasting, J.F. and Traub, W.A. (2010) Exoplanet characterization and the search for life. White paper for Astro2010: The Astronomy and Astrophysics Decadal Survey, Board on Physics and Astronomy, The National Academies, Washington, DC. Available online at http://sites.nationalacademies.org/BPA/BPA_050603#planetarysystems.

Kawahara, H., Matsuo, T., Takami, M., Fujii, Y., Kotani, T., Murakami, N., Tamura, M., and Guyon, O. (2012) Can ground-based telescopes detect the oxygen 1.27 μm absorption feature as a biomarker in exoplanets? *Astrophys J* 758: 13–23.

Köhler, J., Melf, M., Posselt, W., Holota, W., and te Plate, M. (2005) Optical design of the near-infrared spectrograph NIRSpec. *Proc SPIE* 5962:563–574.

Kump, L.R. (2008) The rise of atmospheric oxygen. *Nature* 451:277–278.

Lafreniere, D., Doyon, R., and the FGS/NIRISS, NIRCam, MIRI, and NIRSpec Science Teams. (2013) The science potential of JWST for exoplanet studies [presentation number 135.06]. In *Bulletin of the American Astronomical Society,* Vol. 45, AAS Meeting #221.

Maté, B., Lugez, C., Fraser, G.T., and Lafferty, W.J. (1999) Absolute intensities for the O_2 1.27 μm continuum absorption. *J Geophys Res* 104:30585–30590.

Meadows, V.S. and Crisp, D. (1996) Ground-based near-infrared observations of the Venus nightside: the thermal structure and water abundance near the surface. *J Geophys Res* 101: 4595–4622.

Mitchell, R.M. and O'Brien, D.M. (1987) Error estimates for passive satellite measurement of surface pressure using absorption in the A band of oxygen. *Journal of the Atmospheric Sciences* 44:1981–1990.

Pallé, E., Zapatero Osorio, M.R., Barrena, R., Montañés-Rodríguez, P., and Martín, E.L. (2009) Earth's transmission spectrum from lunar eclipse observations. *Nature* 459:814–816.

Pierrehumbert, R.T. (2010) *Principles of Planetary Climate,* Cambridge University Press, Cambridge, UK.

Pont, F., Knutson, H., Gilliland, R.L., Moutou, C., and Charbonneau, D. (2008) Detection of atmospheric haze on an extrasolar planet: the 0.55–1.05 μm transmission spectrum of HD 189733b with the Hubble Space Telescope. *Mon Not R Astron Soc* 385:109–118.

Rauer, H., Gebauer, S., Paris, P.V., Cabrera, J., Godolt, M., Grenfell, J.L., Belu, A., Selsis, F., Hedelt, P., and Schreier, F. (2011) Potential biosignatures in super-Earth atmospheres. I. Spectral appearance of super-Earths around M dwarfs. *Astron Astrophys* 529:A8–A21.

Rothman, L.S., Gordon, I.E., Barbe, A., Benner, D.C., Bernath, P.F., Birk, M., Boudon, V., Brown, L.R., Campargue, A., Champion, J.-P., Chance, K., Coudert, L.H., Dana, V., Devi, V.M., Fally, S., Flaud, J.-M., Gamache, R.R., Goldman, A., Jacquemart, D., Kleiner, I., Lacome, N., Lafferty, W.J., Mandin, J.-Y., Massie, S.T., Mikhailenko, S.N., Miller, C.E., Moazzen-Ahmadi, N., Naumenko, O.V., Nikitin, A.V., Orphal, J., Perevalov, V.I., Perrin, A., Predoi-Cross, A., Rinsland, C.P., Rotger, M., Šimečková, M., Smith, M.A.H., Sung, K., Tashkun, S.A., Tennyson, J., Toth, R.A., Vandaele, A.C., and Vander Auwera, J. (2009) The HITRAN 2008 molecular spectroscopic database. *J Quant Spectrosc Radiat Transf* 110:533–572.

Seager, S. and Sasselov, D.D. (2000) Theoretical transmission spectra during extrasolar giant planet transits. *Astrophys J* 537:916–921.

Segura, A., Kasting, J.F., Meadows, V., Cohen, M., Scalo, J., Crisp, D., Butler, R.A.H., and Tinetti, G. (2005) Biosignatures from Earth-like planets around M dwarfs. *Astrobiology* 5:706–725.

Segura, A., Meadows, V.S., Kasting, J.F., Crisp, D., and Cohen, M. (2007) Abiotic formation of O_2 and O_3 in high-CO_2 terrestrial atmospheres. *Astron Astrophys* 472:665–679.

Slanina, Z., Uhlk, F., De Almeida, W., and Hinchliffe, A. (1994) A computational thermodynamic evaluation of the

altitude profiles of $(N_2)_2$, N_2-O_2 and $(O_2)_2$ in the Earth's atmosphere. *Thermochimica Acta* 231:55–60.

Spiga, A., Forget, F., Dolla, B., Vinatier, S., Melchiorri, R., Drossart, P., Gendrin, A., Bibring, J.-P., Langevin, Y., and Gondet, B. (2007) Remote sensing of surface pressure on Mars with the Mars Express/OMEGA spectrometer: 2. Meteorological maps. *J Geophys Res (Planets)* 112:8–24.

Uhlik, F., Slanina, Z., and Hinchliffe, A. (1993) Gas-phase association of O_2: a computation thermodynamic study. *Thermochim Acta* 228:9–14.

Vidal-Madjar, A., Lecavelier des Etangs, A., Désert, J.-M., Ballester, G.E., Ferlet, R., Hébrard, G., and Mayor, M. (2003) An extended upper atmosphere around the extrasolar planet HD209458b. *Nature* 422:143–146.

Wakeford, H.R., Sing, D.K., Deming, D., Gibson, N.P., Fortney, J.J., Burrows, A.S., Ballester, G., Nikolov, N., Aigrain, S., Henry, G., Knutson, H., Lecavelier des Etangs, A., Pont, F., Showman, A.P., Vidal-Madjar, A., and Zahnle, K. (2013) HST hot Jupiter transmission spectral survey: detection of water in HAT-P-1b from WFC3 near-IR spatial scan observations. *Mon Not R Astron Soc* 435:3481–3493.

Zerkle, A.L., Claire, M.W., Domagal-Goldman, S.D., Farquhar, J., and Poulton, S.W. (2012) A bistable organic-rich atmosphere on the Neoarchaean Earth. *Nat Geosci* 5:359–363.

Address correspondence to:
Amit Misra
Box 351580
UW Seattle
WA 98195-1580

E-mail: amit0@astro.washington.edu

Submitted 13 February 2013
Accepted 5 December 2013